Environmental Research Center Papers

NUMBER 14

1990

Environmental Research Center
The University of Tsukuba

Large-Scale Air-Sea Interactions in the Tropical Western Pacific on Interannual and Intraseasonal Time Scales*

By Ryuichi Kawamura**

(Manuscript received 30 September 1990)

ABSTRACT

It has recently been recognized that the air-sea coupling in the warm water region of the western Pacific must be better understood since it is identified with triggering the El Nino/Southern Oscillation (ENSO) phenomenon. However, it is still considerably uncertain what air-sea coupled system is essential or prominent for each time and spatial scale. This paper addresses the question of large-scale air-sea coupling in the warm water region of the western Pacific on two time scales; *i.e.*, the interannual and intraseasonal time scales. The following results were obtained:

(1) The interannual variability of the main thermocline in the tropical western Pacific along the 137°E longitude line is reflected primarily in the quasi-biennial oscillation (QBO) time scale. Each dominant eastward-propagating QBO mode is extracted by applying a complex EOF analysis to the sea surface temperature (SST) and 700 mb zonal wind anomaly fields over the tropical Indian and Pacific Oceans. The QBO mode of the SST does not propagate with a uniform phase speed and a marked phase difference is found in the area around 150-160°E, where the eastward-propagating QBO mode of 700 mb zonal wind exhibits uniform phase speed and has the largest amplitudes. It is concluded that the QBO of the upper ocean temperature in the warm water region results from the dynamic response of the ocean to the wind stress having a QBO time scale.

(2) Two air-sea coupled modes; *i.e.*, intraseasonal and interannual modes, are statistically extracted using the complex EOF analysis. There exist remarkable differences in the air-sea coupling of the intraseasonal time scale compared with the interannual time scale. It is found that in the intraseasonal mode, the SST is approximately out of phase with the high-cloud cover (HCC) and 850 mb zonal wind (u). For this mode the region of maximum SST anomaly lies to the east of the center of active convection, which favors the eastward propagation of the large-scale disturbance as well as the evaporation-wind feedback effect. On the other hand, for the interannual mode the SST is almost in phase with the HCC, but the phase relation of the 850 mb u is different in each region of the tropical western Pacific. The predominant growth of this mode defined in the key region (0°-10°N, 130°-160°E) coincides with the life cycle of the ENSO: the occurrence, development and decay.

(3) The growth of the atmospheric 30-60 day oscillation over the equatorial western Pacific is even affected by high SST above a threshold value of 28°-28.5℃. The intraseasonal variations, especially with 40-60 day scales are predominant when the mean SST over the warm water region

---

* A dissertation submitted in partial fulfillment of the requirements for the degree of Doctor of Science in Doctoral Program in the University of Tsukuba

** Present affiliation: Atmospheric and Hydrospheric Science Division, National Research Institute for Earth Science and Disaster Prevention, Tsukuba, Ibaraki 305, JAPAN

is in the range of 29°–29.5℃. There exists strong air–sea coupling on the intraseasonal time scale in the warm water region. Once the tropical western Pacific SST is above the upper threshold value of about 29.5℃, it is clearly seen that the 30–60 day oscillation is damped in this region, although tropical large-scale convection is still rather active. As a result, high frequency fluctuations (*e.g.*, 15–25 day period) become relatively dominant under high SST conditions. The air–sea coupling for the 30–60 day time scale is very weak in this region and disturbances organized on the scale of the super cluster are infrequently observed. Notable eastward–moving air–sea interactive systems on the intraseasonal time scale are not observed.

CONTENTS

LIST OF FIGURES

LIST OF TABLES

LIST OF ABBREVIATIONS

CEOF	complex empirical orthogonal fuction.
CISK	conditional instability of the second kind.
COARE	coupled ocean–atmosphere response experiment.
ENSO	El Nino/Southern Oscillation.
FGGE	first GARP global experiment.
HCC	high-cloud cover.
ITCZ	intertropical convergence zone.
OHC	ocean heat content.
OLR	outgoing longwave radiation.
SPCZ	South Pacific convergence zone.
SST	sea surface temperature.
SWT	sea water temperature.
TOGA	tropical ocean global atmosphere program.
QBO	quasi-biennial oscillation.

CHAPTER I

INTRODUCTION

General aspects

The Tropical Ocean Global Atmosphere (TOGA) program, designed to better understand the physical processes of the tropical ocean-global atmosphere interactive system, has been conducted for about five years a number of meteorologists and oceanographers. However, many scientific problems of coupled ocean-atmosphere systems still remain. Several problems which are not well understood are presented follows (TOGA COARE, 1989):

(1) The heat balance for the warm water region of the western Pacific Ocean is poorly known with discrepancies as large as 80 Wm^{-2}. The relative involvement of the slowly-evolving atmospheric flow (such as the trade-wind regime) and the higher-frequency, more episodic, equatorial events (such as westerly bursts and organized convective phenomena) are not understood.

(2) Theories of El Nino/Southern Oscillation (ENSO) require the instability of, or the oscillation about the basic state of the coupled system. However, maintenance of that basic state and the reasons for the temperature of the warm water lying between 28 and 30℃ with a characteristic broad, low gradient are not well understood. During the warm phase of the ENSO cycle, the warm water region varies by less than 1℃ with much larger changes occurring in the central and eastern Pacific Ocean. It is not clear whether the relatively small changes of the warm water critically influence the atmosphere.

(3) The large-scale time-mean atmospheric divergence coincides with the SST in excess of about 28℃, with the maximum time-mean precipitation, and with centers of convective action as indicated by the variance of outgoing longwave radiation. However, the reasons for these phenomena occurring at the same location are not well known.

(4) Contributions to the long-term averaged moisture divergence by the shorter time-scale variations (*e.g.*, variations on the 30-60 day, 2-6 day and diurnal time scales) are not understood, although there is considerable modeling and observational evidence that suggests interactions and organization across a broad frequency band.

In order to resolve the above problems, it has recently been recognized that the air-sea coupling in the warm water region of western Pacific must be understood, since it is thought to trigger the ENSO phenomenon (*e.g.*, Lau and Chan, 1986; Nitta and Motoki, 1987). It is expected that large-scale cumulus convective activity is very sensitive to small fluctuations of high sea surface temperatures (SST) in this region, although the amplitude of the SST variation is much smaller than those in other regions. However, despite the importance of the air-sea coupled system in the warm water region, it is still not very clear what air-sea coupled system is essential or predominant for each time and spatial scale. In this study focus will be especially concentrated on two time scales; *i.e.*, the interannual and intraseasonal time scales.

Interannual time scale

The SST over the tropical Pacific has the distinct interannual variabilities of the ENSO (4-5 years) and the quasi-biennial oscillation (QBO) time scales (see, *e.g.*, Yoshino and Kawamura, 1987, Yasunari, 1989). The QBO time scale is more periodic than the ENSO time scale. It is also possible that the ENSO may be considered as an amplitude mondulation of the QBO (Lau and Sheu, 1988). The existence of the QBO in the tropical lower troposphere has been confirmed by Trenberth (1975) and others. Yasunari (1985) regarded the QBO as an eastward-propagating mode of the global-scale east-west circulation found in the tropics.

Meehl (1987) noted the biennial tendency of monsoon rainfall in the tropical Pacific and Indian Ocean regions.

Thus, it is suggested that the QBO, especially in the tropical western Pacific, is the important key to understand the air-sea coupled system in the tropics on the interannual time scale. However, it is still uncertain how the tropospheric QBO is coupled with the "oceanic" QBO in the tropics. One purpose of this paper is to investigate the relationships between the tropospheric and oceanic QBOs and to explore a possible air-sea interaction.

Intraseasonal time scale

The importance of the wave-CISK mechanism on the 30-60 day oscillation has been verified by the results of numerical models (Hayashi and Sumi, 1986; Lau and Peng, 1987; Yamagata, 1987, *etc.*). According to Hayashi and Golder (1986, 1988) the tropical zonal velocity of a high resolution Geophysical Fluid Dynamics Laboratory (GFDL) General Circulation Model (GCM) exhibits two intraseasonal wavenumber 1 spectral peaks with periods of 40-50 and 25-30 days. The 40-50 day peak corresponds to the observed intraseasonal oscillations, while the latter peak is related to the simulated intraseasonal oscillations appearing in low resolution GCMs. However, it is still uncertain why the simulated intraseasonal oscillations show a fast eastward-propagation compared with those observed. Takahashi (1987) suggested that the slow speed of the intraseasonal oscillation may be explained by modifying the vertical distribution of convective heating in the wave-CISK mode. More recently, Sui and Lau (1989) concluded that lower boundary forcing due to the heat flux from the ocean surface destabilizes the mobile wave-CISK mode. Miyahara (1987) demonstrated the effect of the sea surface temperature (SST) on tropical convective actibity by varying the CISK parameter with longitude and latitude. Thus, several studies focus on the role of tropical SST as the lower boundary in destabilizing the intraseasonal mode. On the other hand, Emanuel (1987) found that the evaporation-wind feedback mechanism leads to the eastward propagation of intraseasonal disturbances. Furthermore, Neelin *et al.* (1987) suggested that the amplitude of the 30-60 day oscillation is strongly influenced by the evaporation-wind feedback mechanism. However, in a strict sense, air-sea interactions are not considered since the numerical models used in these studies had fixed oceans. Therefore, the need rises to investigate whether or not an air-sea coupled system exists on the intraseasonal time scale.

The existence of oceanic intraseasonal variations (tropical SST, sea leval or current velocity) has already been reported by Mysak and Mertz (1984), Enfield and Lukas (1984), Spillane *et al.* (1987), Schott *et al.* (1988), Kutsuwada (1988), Krishnamurti *et al.* (1988), and others. It has further been found that the tropical SST exhibits a coupling with the outgoing longwave radiation (OLR) having the same time scale with a phase difference of 10-20 days (Murakami, 1988; Kawamura, 1988b). This fact suggests not only the importance of the dependence of the 30-60 day oscillation on the SST, but also the air-sea interaction this time scale. Lau and Shen (1988) by using a simple air-sea coupled model, showed that two Kelvin-like unstable modes; *i.e.*, advective and upwelling modes, exist in the tropical atmosphere-ocean system. Their results reval very intriguing information for understanding the dynamics of intraseasonal oscillations and the ENSO. However, their study used only one example from observations to explain when and how two such modes occur and evolve. Thus, it is necessary to specify the behavior of the two modes by statistically analyzing observational data. Moreover, they insist that the advective and upwelling modes are observed during the onset and mature phases of ENSO, respectively. However, it is not clear how the two modes are associated with the interannual time scale, represented by the ENSO and QBO.

Research Objective

The purpose of this research, therefore, is to explain observationally the air-sea coupling on the intraseasonal time scale which has not been considered and to compare it with that on the interannual time scale. This study focuses on the warm water region of the western Pacific since it is the region of strong intraseasonal oscillations and is also the key region associated with the onset of the ENSO.

A brief description of the global climatology of the SST and OLR fields is given in Chapter 2. Chapter 3 discusses the QBO-like interannual variations appearing in the sea water temperature (SWT) and SST associated with the anomalous east-west circulation in low-latitudes, utilizing time filtering and complex empirical orthogonal function (CEOF) analyses. Chapter 4 presents the intraseasonal variability of large-scale convection and SST. In Chapter 5, the statistically dominant phase relationships among SST, zonal wind at 850mb, and high-cloud cover (HCC) on intraseasonal and interannual time scales are extracted, using CEOF analysis and the air-sea coupling of the two time scales is discussed. Concluding remarks and discussion are found in Chapter 6.

CHAPTER II

GLOBAL CLIMATOLOGY

2.1 Data

Interpolated daily-mean OLR at a resolution of 2.5°latitude-longitude are used for the low and middle latitude region (45°N-45°S), obtained from the original twice daily data for the period 1975-1987 (except 1978) from NMC/NOAA. Also utilized are the global monthly mean SST data at a resolution of 5°latitude-longitude, compiled by the UK meteorological office. The data were extracted for the low and middle latitude region (45°N-45°S) over the period 1950-1988. A more elaborate explanation of the data is given by Parker and Folland (1988).

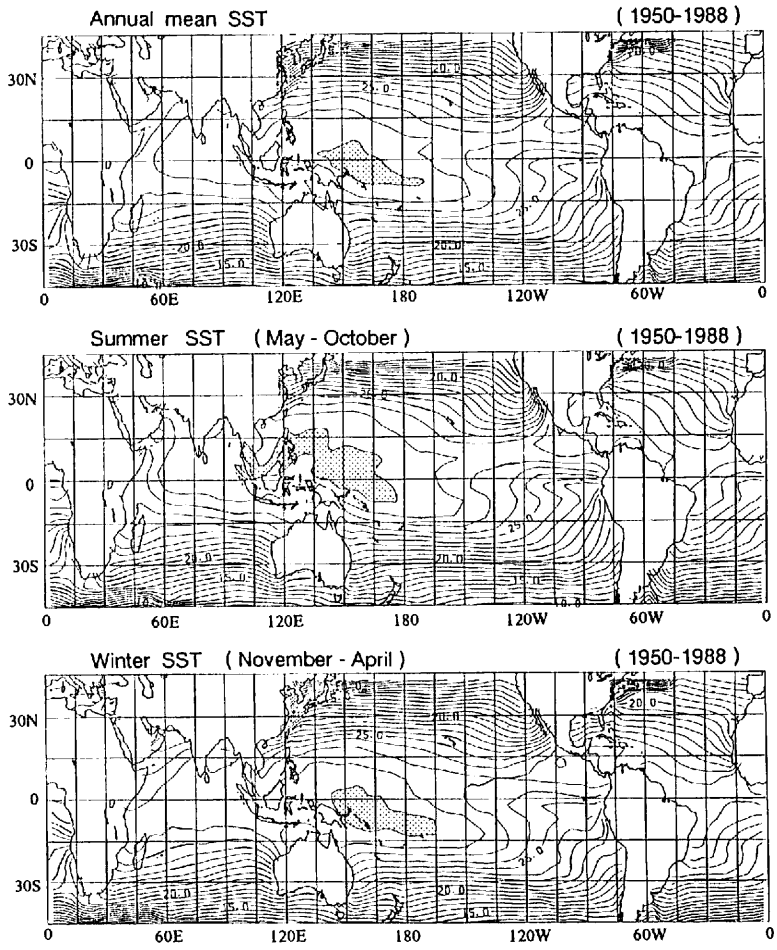

Fig.2.1 Climatological SST field in low and middle latitude regions for (a) annual mean, (b) Northern summer (May-October) and (c) Northern winter (November-April) over the 39-year period from 1950 to 1988. Contour interval is 1℃.

2.2 Sea surface temperature (SST) field

Figure 2.1 shows the climatological SST field in the low and middle latitude regions for (a) the annual mean, (b) the northern summer (May–October), and (c) the northern winter (November–April) over the period 1950–1988. Warm SST areas above 28℃ are found in the tropical western Pacific and tropical Indian Oceans. It can also be seen that the warmest region of SST, greater than 29℃, is confined to the area over the tropical western Pacific, which is called the "warm pool" region. In the warm pool region of the western Pacific, warm water is usually accumulated and the ocean mixed layer is deep, with the main thermocline found at a depth of about 200–300 m near the equator.

2.3 Outgoing longwave radiation (OLR) field

Figure 2.2 displays the climatological OLR field over the low and middle latitudes for (a) the annual

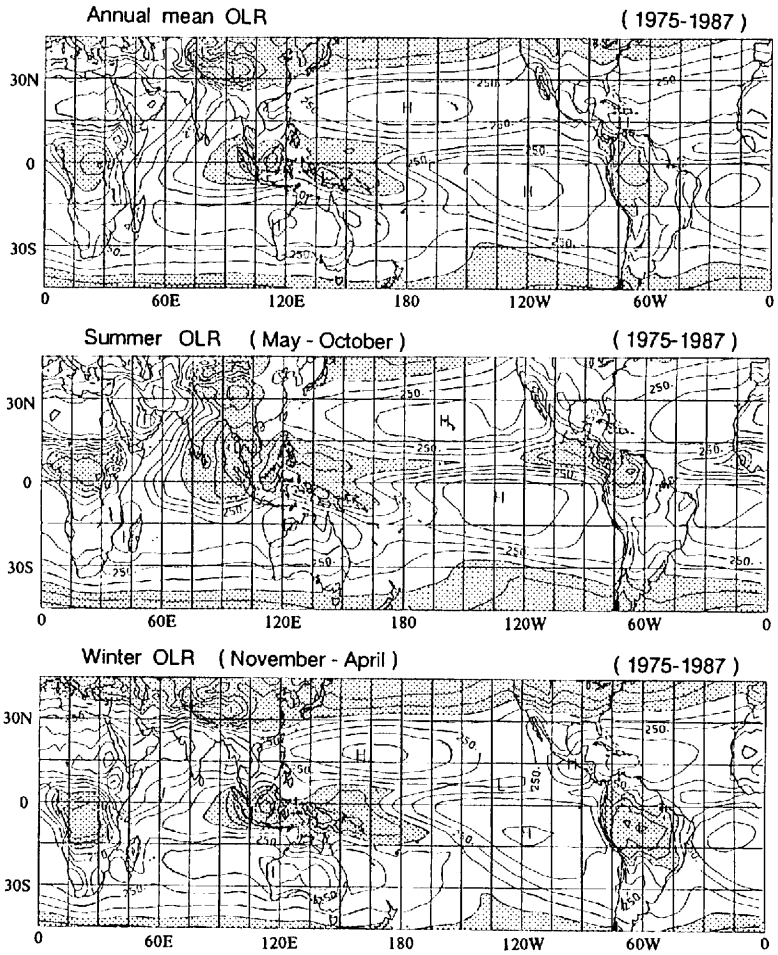

Fig.2.2 Climatological OLR field in low and middle latitude regions for (a) annual mean, (b) Northern summer and (c) Northern winter over the period 1975–1987 (except 1978). Contour interval is 10Wm^{-2}

mean, (b) the northern summer (May–October), and (c) the northern winter (November–April) during the period 1975–1987 (exclusive of 1978). The OLR provides a useful measure of active convection in tropical regions since low values correspond to large amounts of high-cloud cover, indicating the dominance of tropical convection.

Deep Convective regions of less than 240 Wm^{-2} are observed in a belt extending from the tropical Indian Ocean to the western Pacific. It is clearly seen that both the Intertropical Convergence Zone (ITCZ) and the South Pacific Convergence Zone (SPCZ) extend over the tropical Pacific Ocean. It can also be seen that the three largest regions of convective heat source in the tropics are the maritime continent, central Africa, and the northern part of South America. The effects of the maritime continent on large-scale convective activity are more important than those of other regions, since the maritime continent has characteristics of both an ocean and land, while large-scale convection in this area is strongly affected by air-sea interaction. Examination of the maritime continent reveals that some of the most active convection areas occur over large islands located within the maritime continent. The convection over the islands has a distinct diurnal variation generated by orographic and heating effects, which can be termed the island effect. It is found, on the other hand, that the diurnal variation of convection over the warm ocean is not large as that over the islands.

CHAPTER III

INTERANNUAL VARIATIONS APPEARING IN THE TROPICAL SST, SEA WATER TEMPERATURE (SWT), AND ZONAL WIND IN THE LOWER TROPOSPHERE

3.1 Data

Table 3.1 lists the specifications of the data used in this chapter. To investigate the overall features of the interannual variation of the western Pacific SST, monthly-averaged data were utilized. Also, the SWT data along the 137°E longitude line were used, reflecting a meridional fraction of the vertical thermal structure of the mixed layer in the western Pacific. Significant information of the thermal conditions in the mixed layer of the tropical ocean are needed to discuss the origin of the QBO appearing in the tropical SST anomaly field. The SWT data along this longitude line were regularly collected twice yearly, during January and July by the marine observation ship *Ryofu-Maru* of the Japan Meteorological Agency. Since this data has not been time averaged, care should be taken in interpreting the analyzed results. In order to investigate the air-sea interaction with the QBO time scale, the 700mb zonal wind data were utilized as being representative of the lower tropospheric circulation over the low latitudes.

3.2 Analysis procedures

An EOF analysis was used to identify the major modes in the SWT anomaly pattern of the latitude-height section along the 137°E line. The SWT anomaly is evaluated as a departure from the long-term mean over 14 years (1972-1985) for which both the January and July SWT data were available.

A complex EOF (CEOF) analysis extended to a complex-number domain was also performed with the SST and 700mb zonal wind data in order to clarify possible propagating features of the air-sea coupled QBO mode. The results of the usual EOF analysis clearly extract the 0 or π phase difference among different stations, and hence it is a very common technique for investigating phenomena such as a standing oscillation. However, the above technique cannot easily identify propagating phenomena having phase

Table 3.1 Periods of record, time means, spatial resolution, objective regions and sources of the data used in chapter 3.

Data	Period of record	Time mean or interval	Spatial resolution (lat. × lon.)	Objective region	Source
Sea Surface Temperature (SST)	1970-84	Monthly	2° × 2°	Global	NOAA
Sea Water Temperature (SWT)	1967-86	Twice yearly	lat. 0.5-1.0° depth 0-1200m	137°E line (1°S-34°N)	Oceanographical Division, JMA
NMC global wind data	1968-85	Monthly	lat. 3.5°-5° lon. 5°	Global	National Meterological Center (NMC/NOAA)

shifts in space and time. The CEOF analysis, on the other hand, provides time-lag information, which allows the examination of the space-time structure of a quasi-periodic propagating mode. This analysis technique is briefly described as follows. For a more detailed explanation, see Barnett (1983).

Before the CEOF analysis was applied to the data, the frequency component of the QBO mode appearing in the SST and 700mb wind data was extracted using the band-pass time filter (see Murakami, 1979). By using a Hilbert transform, the filtered data are extended to complex variables. The eigenvalue problem of the complex covariance matrix (Hermite matrix) was solved and as a consequence the real eigenvalues along with the complex eigenvectors of $Bm(J)$ are obtained, where m represents the m-th mode and J is a spatial component. Using $Bm(J)$, the amplitude function of $SAm(J)$ and phase function of $SPm(J)$ in the space domain are respectively defined by

$$SAm(J)=[Bm(J)\ Bm^*(J)]^{1/2}, \tag{3.1}$$

and

$$SPm(J)=\tan^{-1}[\mathrm{Im}\ Bm(J)/\mathrm{Re}\ Bm(J)\ ]. \tag{3.2}$$

These two spatial functions denote where each principal mode grows and how it propagates in space. On the other hand, the complex temporal function $Fm(t)$ is given by

$$Fm(t)=\Sigma X(J,\ t)\ Bm(J) \tag{3.3}$$

where $X(J,\ t)$ represents the complex data extended by the Hilbert transform. The amplitude and phase functions in the time domain can be obtained in a similar manner using $Fm(t)$. The above analysis has the advantage of separating plural propagating modes that have similar frequency domains, although the cross-spectral analysis can be used for various wave phenomena.

3.3 Dominant modes of the SWT anomaly field

Figure 3.1 displays the vertical structure of January and July SWT (not monthly means) over 14 years, from 1972 through 1985. The mean depth of the main thermocline (*i.e.*, the layer in which vertical gradient of the SWT is steepest) occurs at about 200–300m near the equator, becomes shallower at depths of 100–150m in the tropics (5–10°N) and then deepens in mid-latitudes. The maximum depth reaches roughly 400–500m near 30–32°N. The standard deviation of the SWT variation has two dominant peaks in space; one representing the thermocline in the tropics, the other that in the mid-latitudes. The latter seems to correspond to the variability of the axis of the Kuroshio Current.

In order to investigate the interannual variability of the SWT anomaly field, a common EOF analysis was applied latitudinally to the January and July SWT data along the 137°E longitude line. Figures 3.2 and 3.3 reveal the spatial anomaly patterns and their temporal variations for the first two EOF modes. The first and second EOF modes account for 24.1% and 10.6% of the total variance, respectively. The spatial structure of the first mode is dominated by a remarkable north-south pattern having opposite phases in tropical and mid-latitude regions. A center of significant anomalies is located in a layer between 100–150m depth at 5–10°N, which is equivalent to the main thermocline in low latitudes. Other anomalies with the same sign as those in the 100–150m depth layer are also found in the surface layer in the tropics and subtropics, although significant anomalies do not exist at a depth of 50m in this latitude zone. This suggests that the SWTs in the surface layer fluctuate in phase with those near the main thermocline. As

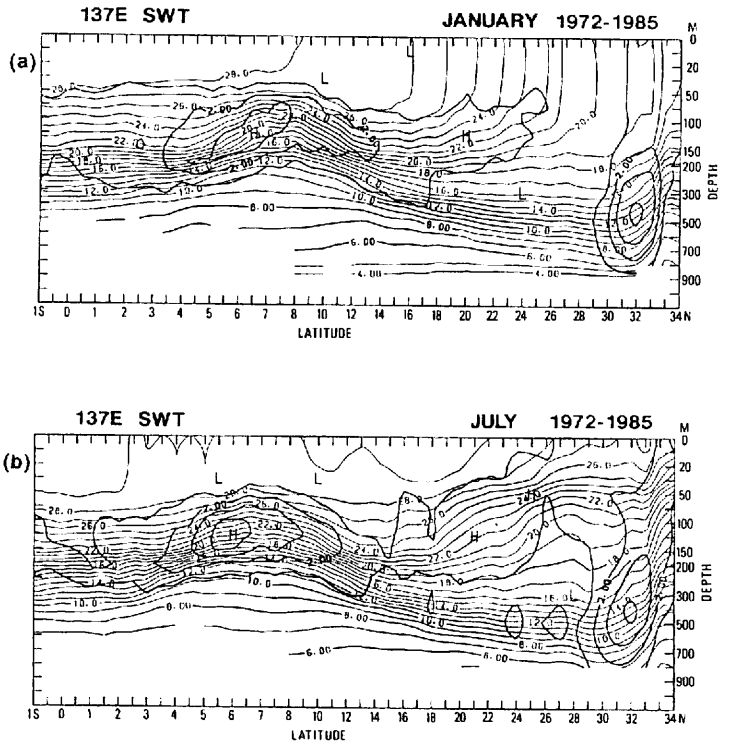

Fig.3.1 Vertical section of sea water temperature (SWT) along 137°E longitude line in January and July during 1972–1985. Contour interval is 1.0℃. The standard deviation is also plotted with a thick line. Note that the scale of depth is not uniform.

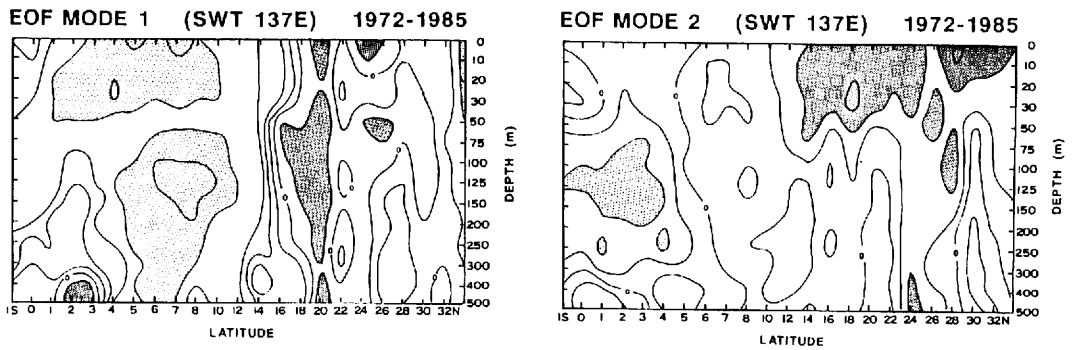

Fig.3.2 Spatial patterns of the first two EOF modes deduced by applying the EOF analysis to the SWT data along 137°E longitude line in January and July during the period 1972–1985. Contours are drawn in relative units. Light and heavy shadings denote areas with marked positive and negative anomalies, respectively.

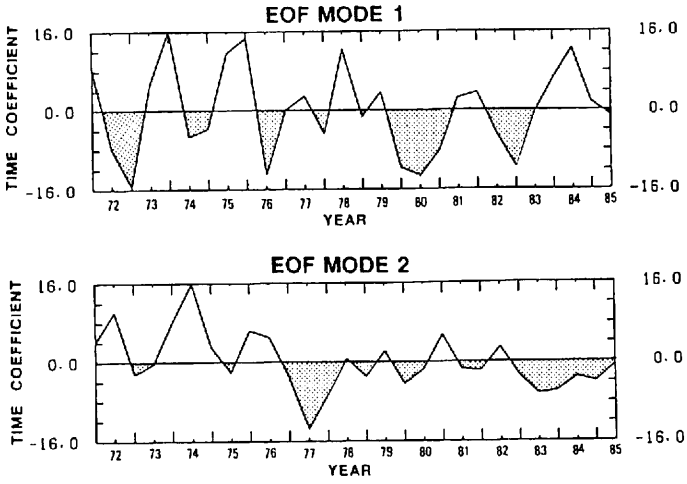

Fig.3.3 Temporal variations (time coefficients) of two EOF modes indicated in Fig.3.2.

shown Fig.3.3, which is composed of twice yearly (January and July) data, it is noteworthy that this mode has an interannual variation with a 2 to 2.5 year period (*i.e.*, the QBO time scale). The variability of the main thermocline in low latitudes must primarily be reflected in the QBO time scale. The QBO-like feature of the tropical SWT was also shown by Yasunari (1988), who discussed the impact of the Indian monsoon on the western tropical Pacific SWT, and by Saiki (1987) who investigated the interannual variation of the subtropical Gyre in the western North Pacific.

In the second mode, negative anomalies are found in the surface layer in the mid-latitudes, while positive anomalies exist in a layer between 100-200m depth in the tropics. The interannual variation is not particularly pronounced in this mode. It appears that the second mode mainly explains thermal conditions of the surface layer above a depth of 50m in the middle latitudes.

3.4 Dominant frequencies of the SST anomaly field

The left panel of Fig.3.4 shows the actual non-seasonal SST fluctuations at the reference points 140°E, 150°E, 160°E, and 170°E along the equator during the period 1979-1984. The band-pass filtered SST fluctuations in the period range 22-28 months at the same points are shown in the right panel. It can be seen that the QBO of the western Pacific SST dominates after 1982 with its maximum amplitude reaching about 1°C, which is a large value for the tropical western Pacific. It is also found that the QBO phase coincides well with the phase of the first EOF mode described in the previous section.

Figure 3.5 shows the time-longitude cross-section of QBO filtered SST anomalies along 20°N, 10°N, and the equator. It is clearly seen that the QBO extends over the western Pacific from the equator to 20°N.

The above features suggest that the QBO is one of the dominant interannual variations of the SST anomaly field over the tropical western Pacific.

3.5 Complex EOF modes of the SST and 700mb zonal wind on quasi-biennial oscillation (QBO) time scales

It is obvious that the QBO-like interannual variability of the SWT anomaly in the main thermocline can be confirmed even in the western tropical Pacific where the variance of the SST is very small. The tropical air-sea coupled QBO involving the Indian Ocean sector is further investigated with respect to the

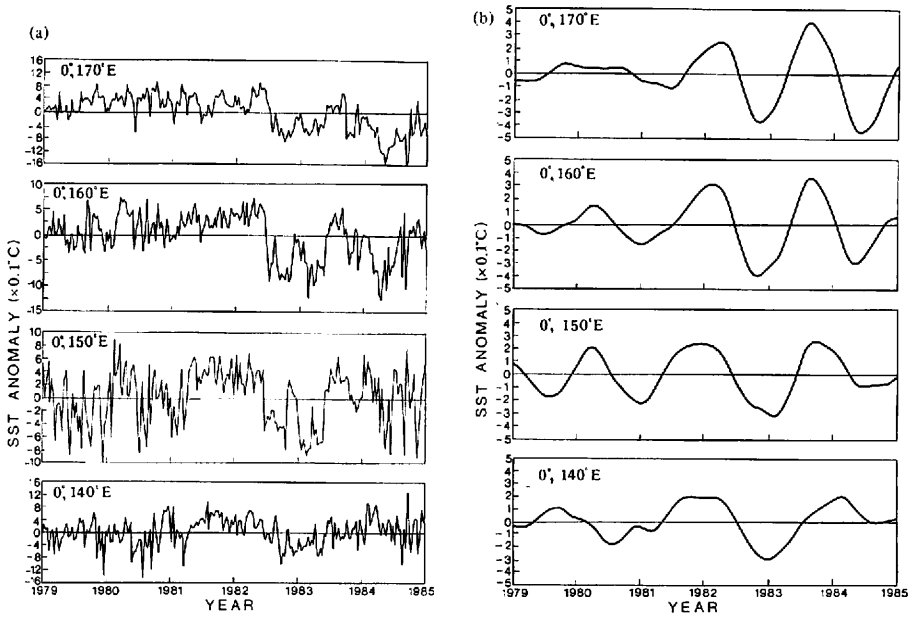

Fig.3.4 (a) Fluctuation of the actual SST at the points 140°E to 170°E along the equator during the period 1979 through 1984 based on the 10-day mean values.
(b) Same as Fig.3.4 (a) but for the filtered SST of the 22-28 month mode (after Yoshino and Kawamura, 1987).

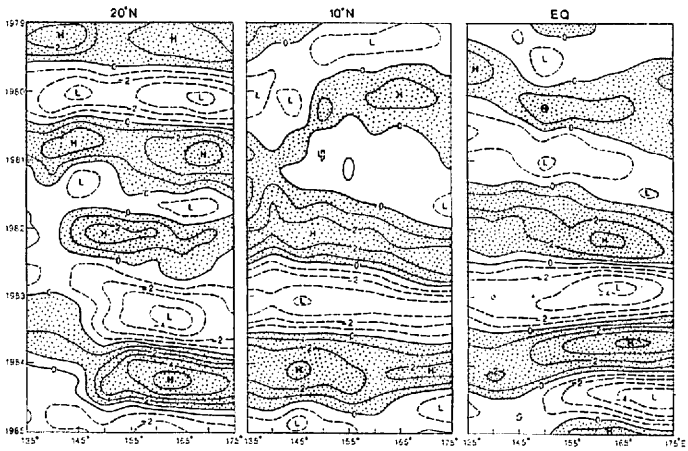

Fig.3.5 Time-longitude cross sections along 20°N, 10°N and the equator of band-pass filtered SST of the 22-28 month mode for 1979 through 1984, Contour interval is 0.1℃ (after Yoshino and Kawamura, 1987).

origin of the SST anomaly in this region.

The spatial amplitude and phase functions of the first CEOF mode in the SST and 700mb zonal wind fields are exhibited in Fig.3.6. Within the amplitude distribution of the SST, there exist regions of somewhat large amplitude not only in the eastern equatorial Pacific, but also in the tropics from the South

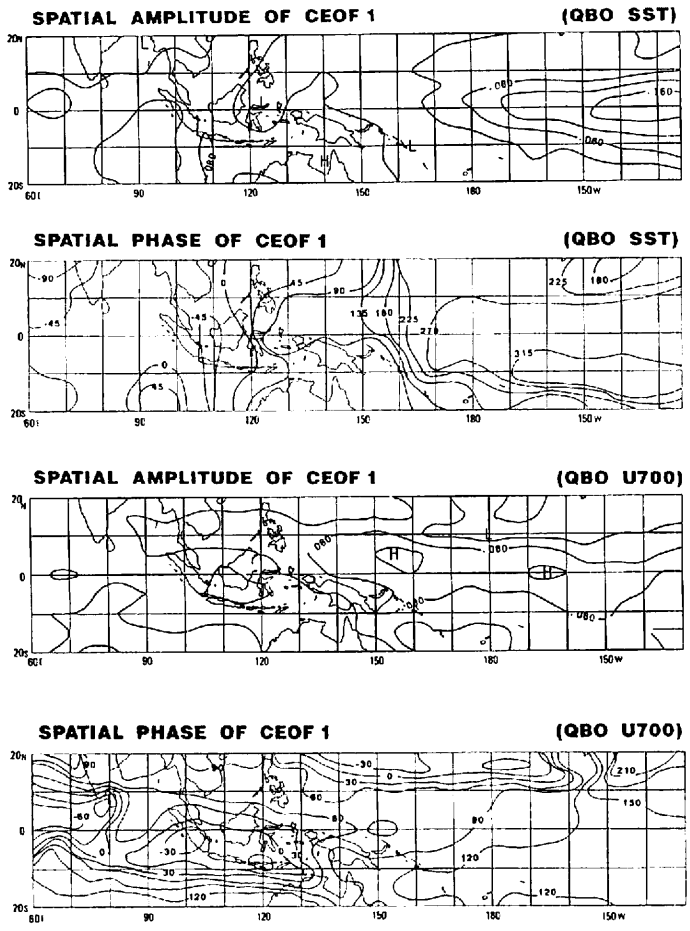

Fig.3.6 Spatial amplitude (relative units) and phase functions (degrees) of the first complex EOF mode of the QBO filtered SST and 700mb zonal wind anomalies.

China Sea to the Indian Ocean. The phase leads primarily in regions west of India and near Borneo, although the regions from the tropical Indian Ocean to South China Sea are roughly in phase, and then propagates from South China Sea, east of the Philippines, across the equator to the eastern Pacific. However, the phase speed is not constant and a pronounced phase gap occurs in the longitude sector 150 to 160°E. The major region of 700mb zonal wind variability, on the other hand, is characterized by a zonally elongated pattern with a maximum amplitude over the western equatorial Pacific near the 150 to 160°E longitude line. The 700mb zonal wind anomalies with a QBO component propagate from the tropical Indian Ocean and the southwest maritime continent eastward over the equatorial regions.

To demonstrate the zonal propagation feaures with seasonal variations, both the SST and the 700mb zonal winds were reconstructed by using only the first CEOF mode such that

$$X(J, t) = F_1(t)\, B_1{}^*(J). \tag{3.4}$$

Next, composites were formed with reference to the 700mb zonal wind anomaly values reconstructed a

key region (0°-10°N, 150°-160°E), where a maximum amplitude in the 700mb zonal wind exists. One QBO cycle is composed of Categories 1 through 8. Category 3 denotes a westerly (positive) maximum phase in the key region, while Category 7 implies an easterly (negative) maximum phase. Other Categories correspond to intermediate phases. Composited anomaly maps of the 700mb zonal wind for Categories 1 through 4 are shown in Fig.3.7. Composited anomaly maps for Categories 5 through 8 are omitted since they are equivalent to the composited maps for Categories 1 through 4 except with the opposite sign. Composited SST anomaly maps are also constructed with reference to the Categories of the zonal wind at 700 mb and are indicated as such in Fig.3.8.

For Category 1 of the 700mb zonal wind, there exist positive (westerly) anomalies from the tropical Indian Ocean to the maritime continent, while negative (easterly) anomalies are observed over the tropical eastern Pacific. Examination of Category 2 shows regions of westerly anomaly propagating eastward and covering the maritime continent and the western Pacific. Category 2 of the SST, however, shows weak negative anomalies in the tropical eastern Pacific, although westerly anomalies appear over the western Pacific. For Category 3, which closely corresponds to June through August, westerly anomalies develop, reach their maximum around 150°-160°E in the tropics and extend further eastward over the tropical Pacific Ocean. On the other hand, very pronounced positive SST anomalies appear in the tropical eastern

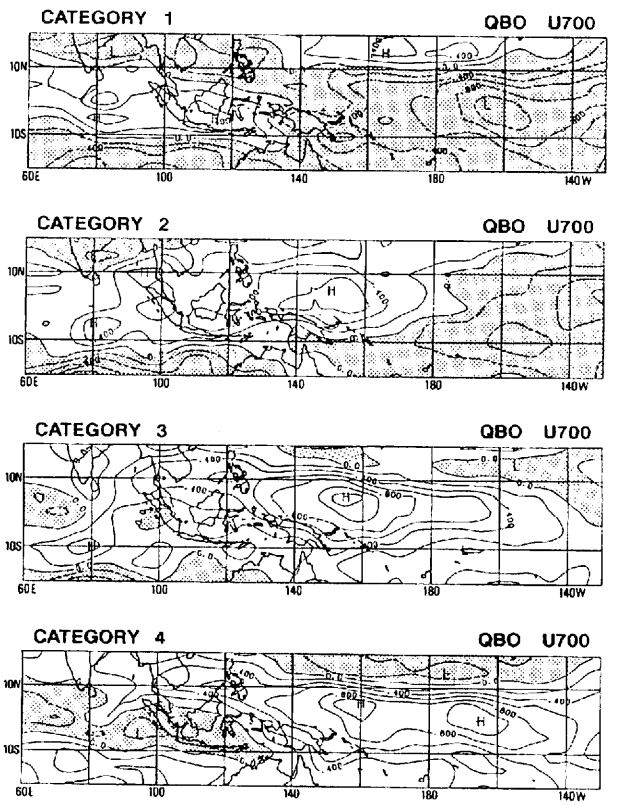

Fig.3.7 Each category of QBO filtered 700mb zonal wind anomalies reconstructed only by the first CEOF mode. Contour interval is 0.2m/s. Negative values are shaded and imply easterly anomalies.

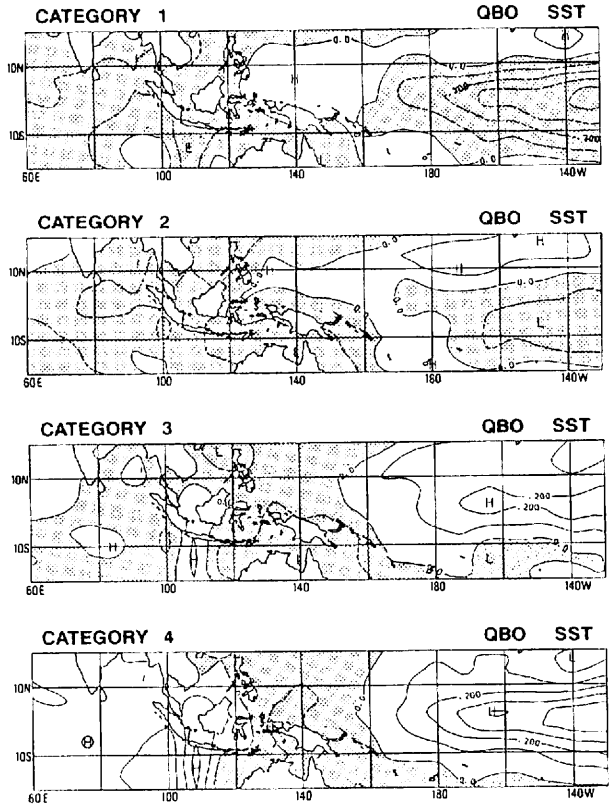

Fig.3.8 Each category of QBO filtered SST anomalies reconstructed similar to Fig.3.7. Contour interval is 0.1℃ and negative values are shaded.

Pacific, whereas negative anomalies are found in the western Pacific. After Category 3, regions of large westerly anomalies move toward the eastern Pacific while easterly anomalies are gradually established over the tropical Indian Ocean and the maritime continent. The positive SST anomalies are intensified over the eastern Pacific.

Figure 3.9 displays the time-longitude cross section of QBO-filtered zonal wind anomalies at 700mb along the equatorial zone (0°-10°N), reconstructed using only the first CEOF mode. Although a discontinuity in the phase appears at 80°E, it can be seen that zonal wind anomalies east of this longitude propagate eastward with a nearly uniform phase speed. Large amplitude modulations of these anomalies are conspicuous over the equatorial Pacific east of the Philippines. Maximum anomalies appear during two periods, from 1973 through 1976 and from 1980 through 1983. This QBO mode is nearly phase-locked to the seasonal cycle and shows maximum amplitudes over the regions from 140 to 160°E, where the variance of the anomaly is largest among areas along the latitude belt, during the warm season from May to October. It appears that the first CEOF mode obtained in the present study accounts for the more fundamental QBO mode propagating eastward with an unchanging phase speed than that at the same 700mb level presented by Yasunari (1985).

The time-longitude cross-section of QBO-filtered SST anomalies along 2 to 10°N is also indicated in

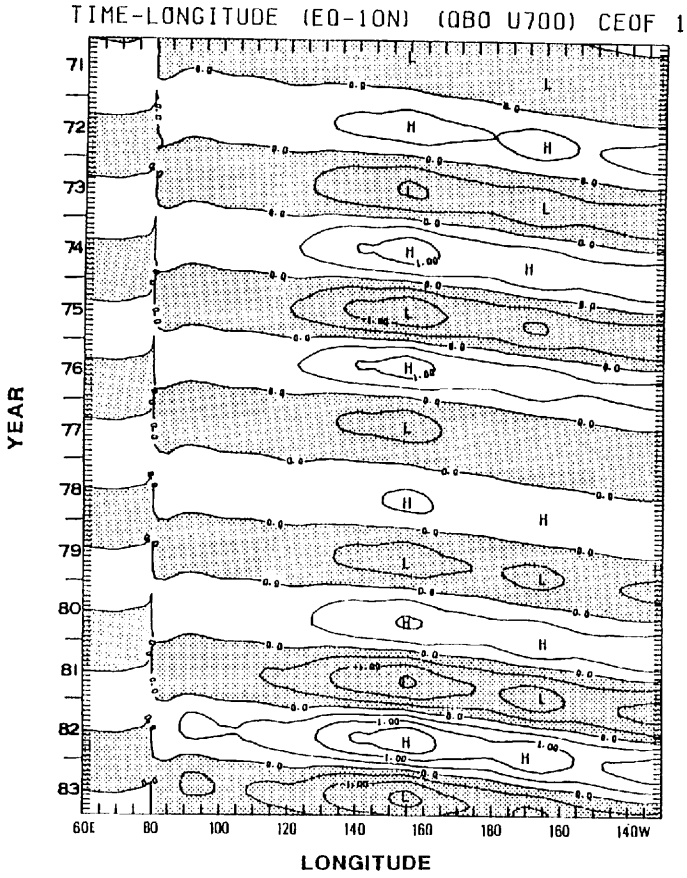

Fig.3.9 Time-longitude cross section of QBO filtered 700mb zonal wind anomalies (0°–10°N) reconstructed only by the first CEOF mode. Contour interval is 0.5m/s and positive values imply westerly anomalies.

Fig.3.10, which is similar to Fig.3.9. The periods of large amplitude almost coincide with those of the 700mb zonal-wind anomaly field. However, the phase speed of the SST anomalies is not uniform and phase differences are observed, most significantly in the regions from 120 to 130°E (corresponding to the Philippines) and from 150 to 160°E. Compared with Fig.3.9, it is found that the area around 150–160°E, where a marked phase shift in the SST anomalies exists, agrees well with the large amplitude area of the 700mb zonal wind anomaly field. When westerly (easterly) anomalies at longitudes around 150–160°E east of the Philippines predominate from May to October, the SST anomalies centered at 140°E have negative (positive) values. These SST anomalies have a prevailing tendency to reach maximum amplitudes about three months later.

The above results suggest that a dominant eastward-propagating QBO mode, which may be a type of normal mode of the tropical troposphere, does not always propagate in parallel with the QBO mode of the SST. Although natural interactions exist between the tropospheric and oceanic QBOs, it can be considered that the pronounced phase shift of the SST anomalies near 150–160°E primarily results from the forcing due to the anomalous wind stress having a QBO variability. Because the QBO mode of the 700mb zonal wind propagates eastward from the tropical Indian Ocean as in Fig.3.9, it is difficult to think that the

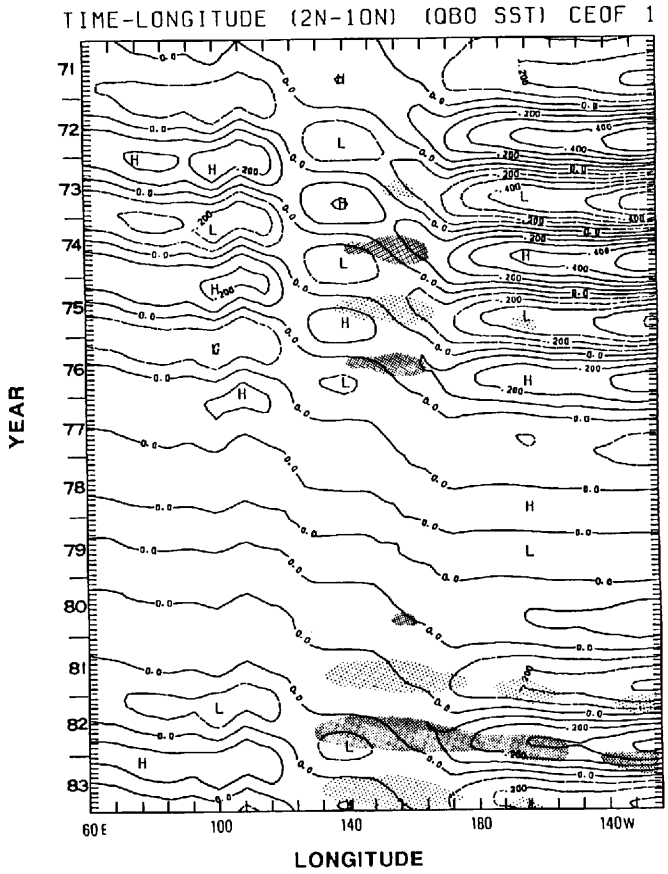

Fig.3.10 Time-longitude cross section of QBO filtered SST anomalies (2–10°N) reconstructed similar to Fig.3.9. Contour interval is 0.1℃. Light and heavy shadings denote areas with easterly and westerly anomalies at the 700mb level more than 1.0m/s.

zonal wind field at the 700mb level over the Indian Ocean is directly influenced by the thermal forcing of the ocean, accompanied by the marked phase shift of the SST anomalies around 150–160°E . Since the SST anomalies around the 137°E longitude line as seen in Fig.3.10 correspond to the time coefficients of the first EOF mode of the SWT anomaly, it is suggested that the QBO modes of the SST and SWT are identical. Thus, it is expected that the SWT anomaly in the main thermocline at low latitudes, which has a QBO-like feature, results from the dynamic response of the ocean to the wind stress having a QBO mode. This idea is also supported by the results of Yasunari (1988). Nitta and Motoki (1987) emphasized the westerly bursts accompanying equatorial twin cyclones as a trigger of El Nino events. The eastward-propagating QBO mode in the lower troposphere may play an important role in producing favorable conditions for the occurrence of the westerly burst over the western Pacific. If this is true, it is deduced that the tropospheric QBO mode presented in this paper affects the onset of the ENSO.

Pronounced SST anomalies over the South China Sea during the cold season, on the other hand, are presumably not formed by the above process. It is found that these anomalies are sensitive to major cold surges (Hanawa et al., 1988; Kawamura, 1988a). Since the cold surge plays a role in intensifying convec-

tive activity in low latitudes when noting their high-frequency variations (*e.g.*,Chang and Lim, 1985; Wang and Murakami, 1987), it is also necessary to investigate the effect associated with the enhanced air-sea coupling of the QBO mode.

CHAPTER IV

INTRASEASONAL VARIABILITY OF LARGE-SCALE CONVECTION AND SST

4.1 Data

The FGGE IIIb global daily data at a low resolution of 11.25° latitude-longitude for 1979 are used, which had previously been rearranged by the Florida State University. Two types of SST data sets are utilized. One is 10-day averaged SST data at a resolution of 1° latitude-longitude over the tropical western Pacific (0°-10°N, 130-179°E), available from data regularly collected by the Japan Meteorological Agency. The other set is the monthly-mean SST data constructed by the UK meteorological office. OLR data are also used, which had previously been explained in Section 2.1. In this chapter, further use is made of the Geostationary Meteorological Satellite (GMS) high-cloud cover (HCC) data defined as a fractional ratio of cloud pixels over a 1° latitude by 1° longitude area, where the top height is above 400 mb. The HCC data provide a measure of active convection similar to the OLR data. The maximum value of HCC is 10.0.

4.2 Analysis procedures

Heat budget analysis

Using the FGGE IIIb data, the large-scale diabatic heating Q_1 and apparent moisture sink Q_2 are given as follows:

$$Q_1 \equiv c_p(p/p_0)^k \left(\partial\theta/\partial t + \boldsymbol{u}\cdot\nabla\theta + \omega\,\partial\theta/\partial p\right), \tag{4.1}$$

and

$$Q_2 \equiv -L\left(\partial q/\partial t + \boldsymbol{u}\cdot\nabla q + \omega\,\partial q/\partial p\right), \tag{4.2}$$

where θ denotes the potential temperature, q the specific humidity water vapor, p the pressure, c_p the specific heat of air at constant pressure, L the latent heat of condensation, ω the vertical p-velocity, $k=R/c_p$, *and* p_0 the reference level (1000 mb).

The vertical p-velocity ω, based on the vertical integration of the continuity equation, is computed as follows (Fig.4.1):

$$\omega(p) = \omega(p_0) - \int_{p_0}^{p} \nabla \boldsymbol{u}_p \, dp \tag{4.3}$$

Here, it is assumed $\omega = 0$ at the 1000 mb and 200 mb levels and a linear correction is made to the horizontal wind divergence, increasing with height.

Spectral analysis

The power spectrum is computed using the Maximum Entropy Method (MEM). The MEM has a useful advantage of high resolution for short data length compared with the other spectral analysis methods. We apply the MEM to the daily OLR data during six months of each year from which the seasonal trend was subtracted, and compute the integrated spectra of OLR for 15-25 day, 30-45 day, and

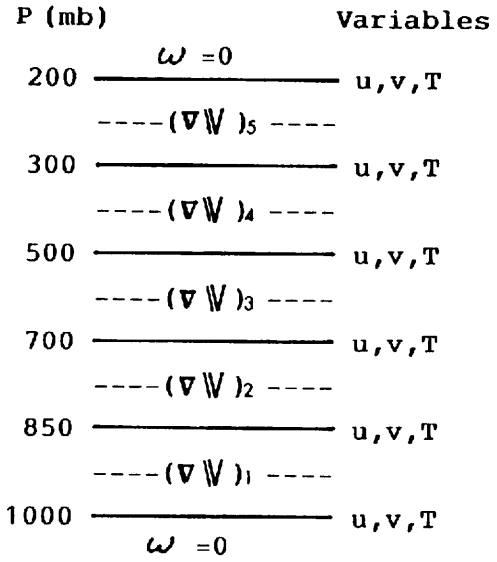

Fig.4.1 Schematic diagram of vertical resolution of the data used for computing vertical p–velocity.

40–60 day period ranges.

4.3 Power spectra of OLR on the intraseasonal time scale

Figure 4.2 shows the layer-averaged diabatic heating Q_1 (K day^{-1}) estimated for the (a) 300–500 mb, (b) 500–700 mb, (c) 700–850 mb and (d) 850–1000 mb layers over the tropical western Pacific sector (6–16°N, 120°E–180°) for 1979. The diabatic heating is larger in the 300–500 mb and 500–700 mb layers. It is clearly seen that the diabatic heating has a remarkable intraseasonal variation with a 30–60 day time scale from May to October 1979. The amplitudes of this variation are about 1–1.5 K day^{-1}. Figure 4.3 shows the layer-averaged apparent moisture sink Q_2 (K day^{-1}) estimated for the (a) 300–500 mb, (b) 500–700 mb, (c)700–850 mb and (d) 850–1000 mb layers for 1979. The apparent moisture sink in the 500–700 mb and 700–850 mb layers has an intraseasonal variation with a 30–60 day time scale and is in phase with the diabatic heating, although its variation is not as clear as that of the diabatic heating.

In tropical convective regions, a large part of the diabatic heating in the middle and upper troposphere appears to be dominated by large-scale convective heating. This is consistent with the above facts, and it can be inferred that tropical convection over the western Pacific varies with the 30–60 day time scale.

Figure 4.4 displays the spatial distributions of integrated power spectra of OLR for the 40–60 day and 30–45 day period ranges for the northern summer (May to October) over the period from 1975 through 1987 (except 1978). Major areas of large power of the 40–60 day fluctuation are observed over the Indian Ocean and the tropical western Pacific. It should be noted that there exist regions of dominant power greater than 150 W^2 m^{-4} over the South China Sea and east of the Philippines. These regions almost coincide with areas where the SST is higher than about 28.5℃, as seen in Chapter 2. Weak power areas are also observed along the ITCZ and the SPCZ. The 30–45 day integrated power spectra distribution has similar overall featuers as the 40–60 day fluctuation, although the mean power is somewhat small.

Another prevailing feature in these figures is that the 30–60 day OLR oscillation is confined to areas only over the tropical Ocean. It should be noted that over the Indian continent, southeast Asia, and the maritime continent notable power of the 30–60 day oscillation is not found. The oscillation shows no

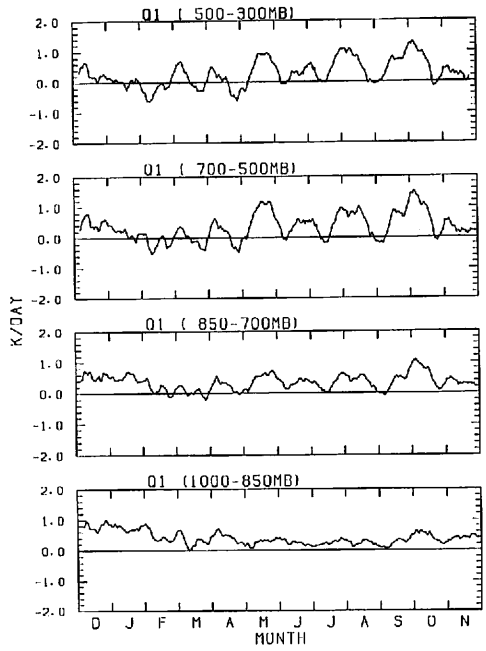

Fig.4.2 Time series of the diabatic heating rate Q_1 ($Kday^{-1}$) computed for the (a) 300–500mb, (b) 500–700mb, (c) 700–850mb and (d) 850–1000mb layers over the tropical western Pacific region (6–16°N, 120°E–180°) for the FGGE year.

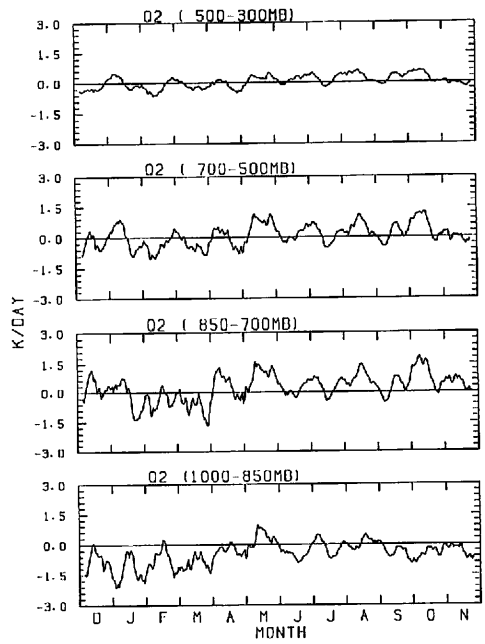

Fig.4.3 As in Fig.4.2, but for the apparent moisture sink rate Q_2 ($Kday^{-1}$).

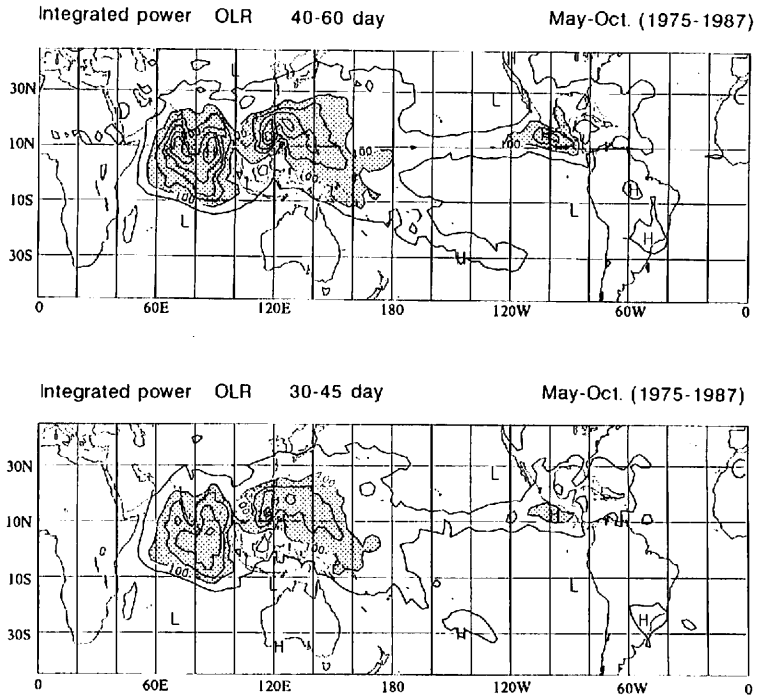

Fig.4.4 Spatial distributions of integrated power spectra of OLR for 40–60 day and 30–45 day period ranges for the Northern summer (May to October) over the period from 1975 through 1987 (except 1978). Contour interval is 50 W^2m^{-4}.

dominance over central Africa and the northern part of South Africa, where convective heating is very large. That is, the observed 30–60 day OLR oscillation tends to be supperssed over land. Furthermore, the oscillation is presumably disturbed over the maritime continent by the island effect mentioned in Chapter 2. This suggests that the 30–60 day oscillation is basically one of the atmospheric low-frequency phenomena that develop over warm oceans.

On the other hand, shown in Fig. 4.5 are the integrated power spectra for the Southern Hemisphere summer (November–April). The large amplitude area shifts to the Southern Hemisphere and predominant peaks are observed over Indian Ocean around (5°S, 80°E) and within the SPCZ. In the Northern Hemisphere winter the deepset convective areas are located around Borneo and New Guinea, as described in Chapter 2. The area of large power for the intraseasonal oscillations, however, is not found over the maritime continent.

The 30–60 day oscillation has a significant overall feature of interannual variability as represented by the amplitude modulation. Figure 4.6 is a bar diagram which indicates the sum of integrated power of the OLR for the 30–45 day the 40–60 day period ranges. Here the integrated power for the northern summer of each year is averaged over the tropical western Pacific sector (0°–10°N, 130–160°E). Over the western pacific it is seen that intraseasonal variations on the 30–60 day scale dominate, especially during the northern summers of 1976, 1979 and 1987, but are not apparent in those of 1975, 1981 and 1983. Figure 4.7 exhibits the integrated power spectra of OLR for the two period ranges for the northern summer of 1979, when the intraseasonal oscillation is prominent over the equatorial western Pacific. The largest values for both periods occur over the South China Sea, slightly west of the Philippines while considerable powers is

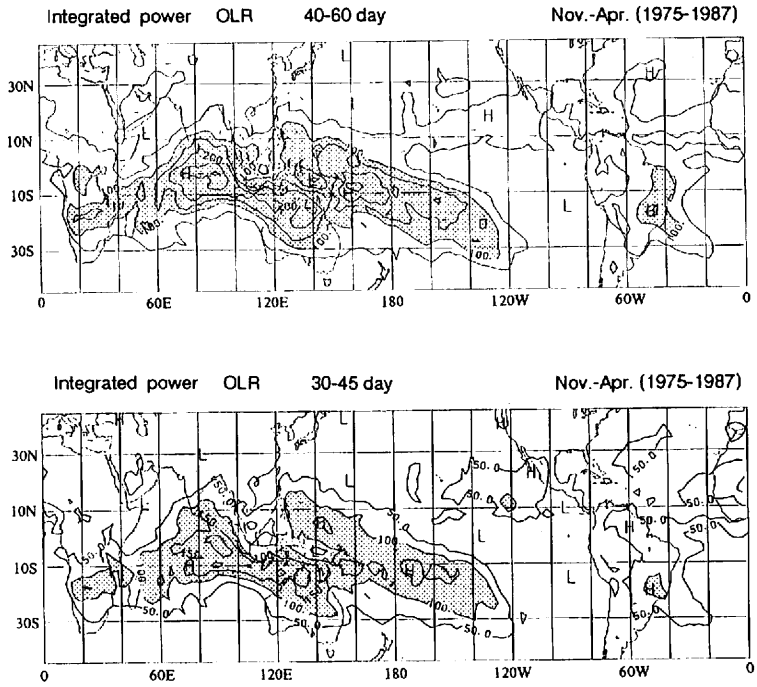

Fig.4.5 As in Fig.4.4, but for the Southern summer (November–April).

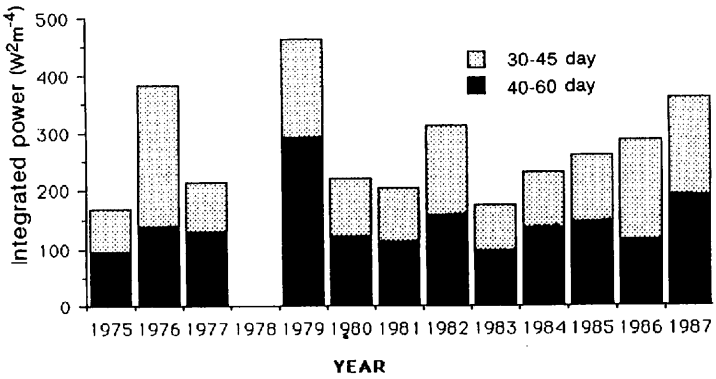

Fig.4.6 Bar diagram of integrated power for the Northern summer of each year averaged over the tropical western Pacific sector (0°–10°N, 130–160°E). Note that the bar is the sum of integrated powers of OLR for the 30–45 day and the 40–60 day period ranges.

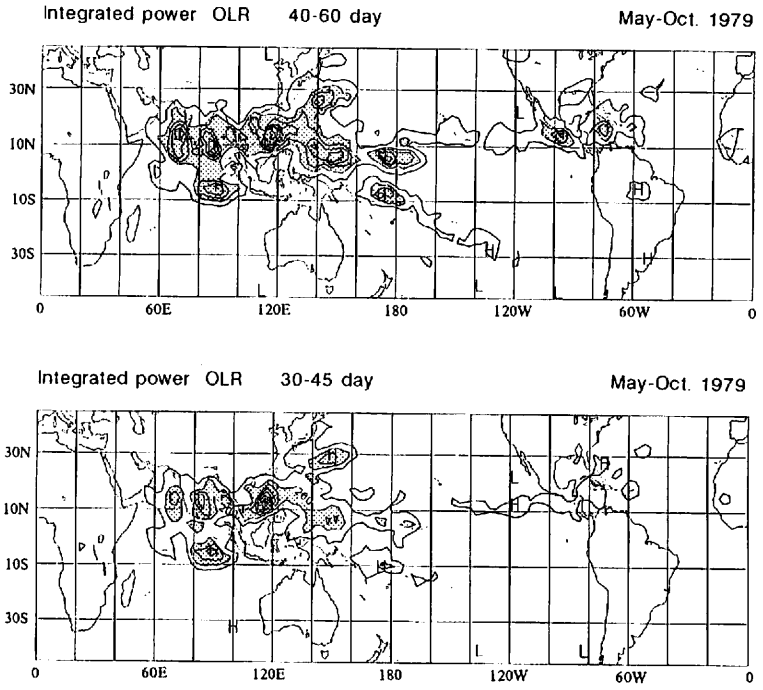

Fig.4.7 Spatial distributions of integrated power spectra of OLR for 40–60 day and 30–45 day period ranges for the Northern summer of 1979. Contour interval is 100 W^2m^{-4}.

seen in the western Pacific region from east of the Philippines though the date line. Nakazawa (1986) examined the filtered anomalies of OLR in the period band of 30–60 days and showed similar features. In contrast, during May–October 1981 (Fig. 4.8), areas of distinct power are not observed over the equatorial western Pacific, while large amplitudes occur at very low latitudes of the Indian Ocean region. It should be emphasized that during this period the SST in the warm pool region of the western Pacific is the warmest of all the analyzed periods (1974–1989), which will be discussed more fully in later sections.

4.4 Dependence of the 30–60 day oscillation on the SST

In the above section, it was shown that large power of OLR in the intraseasopnal time scale is confined to within the tropical Indian Ocean and western Pacific. This is due to the fact that warm SST exceeding about 28℃ is a necessary condition for the active generation of organized deep convection, as was seen in Fig. 2.1. There is a consensus that the relationship between tropical convection and SST is poor when the SST is above threshold values of about 28℃. Gadgil *et al.* (1984) examined the correlation between cloudiness intensity and the SST over the Indian monsoon region for June to September 1966–1972 and concluded that a warm SST is a necessary but not sufficient condition for maintained cloudiness on a monthly basis (as seen in Fig. 4.9). Furthermore, Graham and Barnett (1987) investigated the interrelation between the SST and OLR over the Indian and Pacific Oceans using monthly data for 1974–1979 and, as shown in Fig. 4.10, obtained results similar to those of Gadgil *et al.* (1984). The above intriguing results suggest that beyond the threshold SST, moisture convergence rather than SST plays the dominant role in governing large-scale convection.

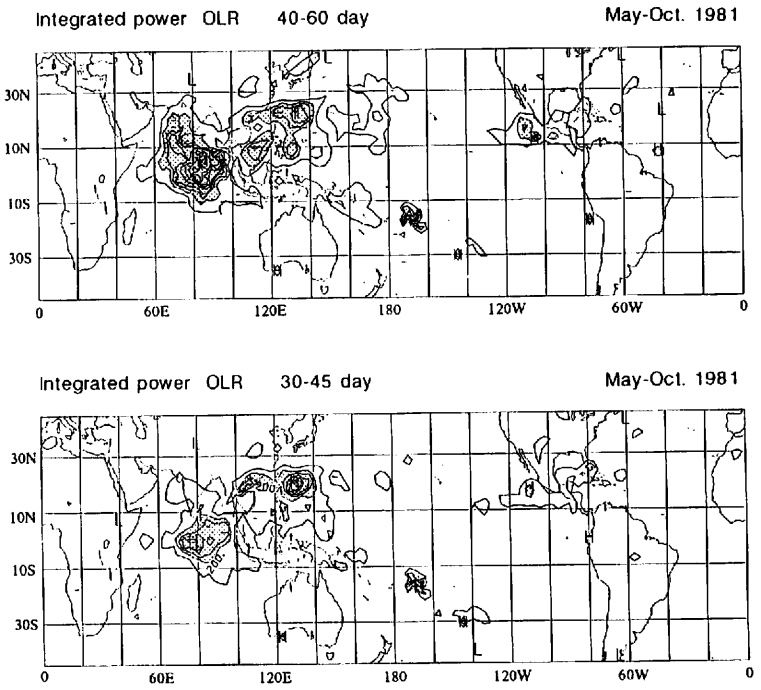

Fig.4.8 As in Fig.4.7, but for 1981.

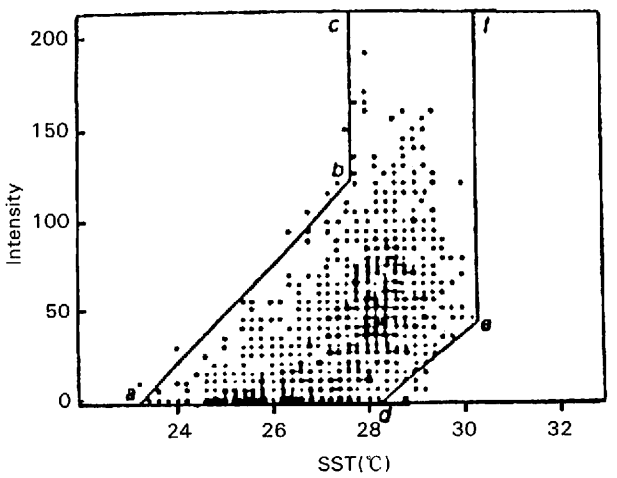

Fig.4.9 Cloudiness intensity plotted against SST for June–September 1966–1972. The number of cell-months at each location is indicated: •, 1–4; ●, 5–9; ⬤, >10 (after Gadgil *et al.* ,1984).

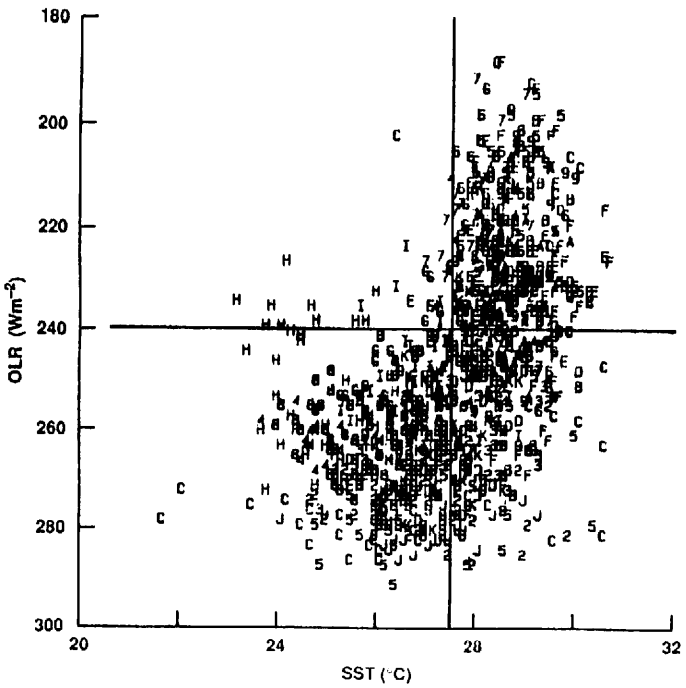

Fig.4.10 Scatter plot of SST and OLR. OLR values decrease (convection increases) toward the top; SSTs are warmer to the right. Note the break at SSTs of~27.5℃ (vertical line) that is associated with OLR values of~240Wm^{-2} (horizontal line), a threshold often associated with deep convection. Also note that there is little relation between SSTs and OLR when SSTs exceed 27.5℃. These are monthly data for 1974 to 1979. Separate symbols are used to represent different locations. The site at 15°N, 50°E is not included (after Graham and Barnett, 1987).

It is therefore expected that the growth of the 30–60 day large-scale disturbance is independent of the SST fluctuation exceeding a threshold value. In fact, it has been emphasized that the 30–60 day oscillation in tropical convection is basically an atmospheric phenomenon, which is excited by the dynamics of the tropical atomosphere, and therefore this oscillation was not regarded as being an air-sea coupled system (*e.g.*, see Hayashi and Sumi, 1986; Lau and Lau, 1986; Hayashi and Golder, 1986; Lau and Chan, 1988). This was concluded from the fact that the intraseasonal oscillation was fairly well simulated using numerical models in which the SST prescribed. However, the above idea has little validity with respect to observational evidence.

To examine whether or not the 30–60 day oscillation is due to the SST if it has temperatures beyond a threshold value of about 28℃, the equatorial western Pacific region was divided into five blocks (10° latitude by 10° longitude) as illustrated in Fig. 4.11. The monthly-mean OLR and SST were averaged over each region and are used for analysis.

Figure 4.12 shows the critical relationships between the SST and integrated power spectra of OLR for

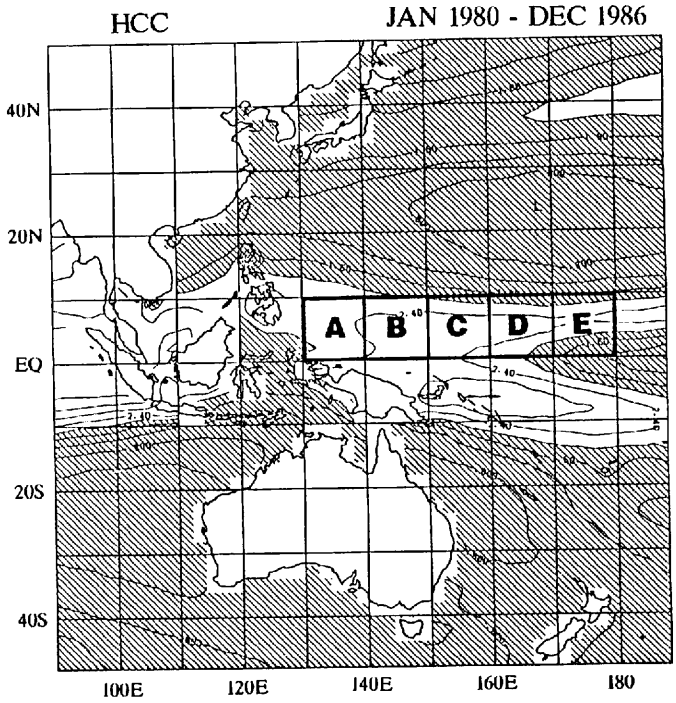

Fig.4.11 Climatological mean HCC field over western Pacific during the 7-year period from 1980 to 1986. Contour interval is 0.40. Location of the five regions selected in this study are also shown.

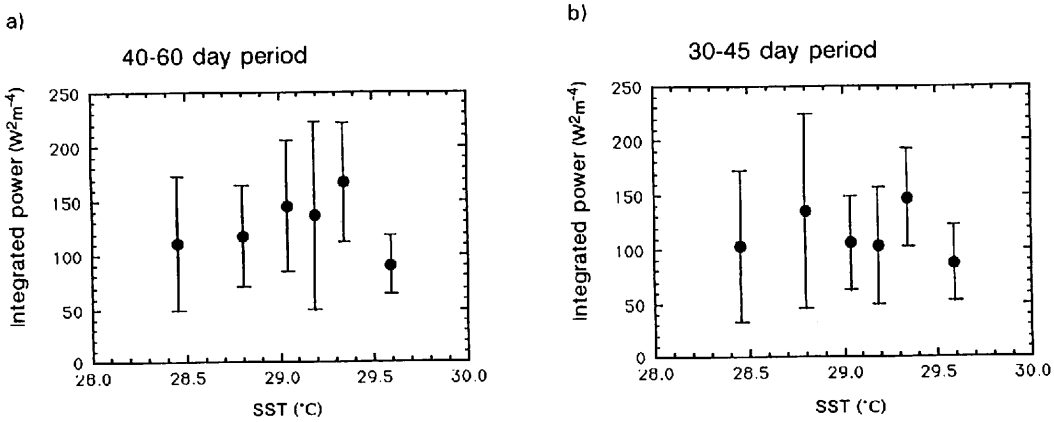

Fig.4.12 Relationships between SST and integrated power spectra of OLR for the 40–60 day period (left panel) and the 30–45 day period (right panel) ranges in Regions from A to E and during the Northern summer (May–October), where the SST values are arranged in ascending order of magnitude and distributed into 6 classes, following which mean and standard deviation values of OLR are plotted for corresponding mean SST of each class.

the 40–60 day period (left panel) and the 30–45 day period (right panel) ranges over the regions from A to E during the northern summer (May–October). The SST values are arranged in ascending order of magnitude and divided into 6 classes, with the mean and standard deviation values of the OLR power plotted for the corresponding mean SST of each class. The left panel of this figure indicates that an increase in the SST tends to increase the power integrated over 40–60 days in the SST range between 28.5° to 29.3℃, whereas a much larger power reduction occurs beyond about 29.5℃. On the other hand, for the 30–45 day period, two dominant peaks of integrated power exist around 28.8° and 29.3℃, while the smallest power occurs beyond about 29.5℃.

Therefore, it is found that over the equatorial western Pacific during the period from May to October, the 30–60 day oscillation predominates under the lower boundary condition that the SST value is around 29.3℃. Moreover, the 30–60 day oscillation tends to dissipate beyond the critical value of about 29.5℃. These results show that the tropical western Pacific SST has the potential to create a critical impact on the 30–60 day oscillation, and therefore the depelndence of this oscillation upon SST should be considered even when the SST is beyond threshold values of about 28℃. Another feature of this figure is that the standard deviation of the integrated power spectra is considerably large. This reflects a well-known fact that moisture convergence due to the CISK mechanism plays a crucial role in developing the 30–60 day disturbance. However, as a secondary effect, it cannot be denied that the SST variations beyond 28.5℃ have a substantial influence on the growth of the 30–60 day wave.

The left panel of Fig. 4.13 shows the ratio of integrated power for the 30–45 day period to that for the 40–60 day period. It is seen that, when the SST is below 29℃, the power for the 30–45 day fluctuation is somewhat greater than that for the 40–60 day fluctuation, a fact which may suggest that the higher-frequency fluctuation (period from 30 to 45 days) is amplified when the SST is below 29℃. On the other hand, the right frequency fluctuation (period from 40 to 60 day) is amplified when the SST is at or above 29℃. It should be noted, however, that both fluctuations are barely sustained when the SST exceeds critical values of 29.5℃. The right panel of this diagram shows the proportion of power integrated from 15–25 days to that from 40–60 days. As was seen in Fig. 4.12, since a much larger power reduction in the 40–60 day fluctuation occurs beyond about 29.5℃, the 15–25 day fluctuation is more dominant where the SST is in excess of 29.5℃.

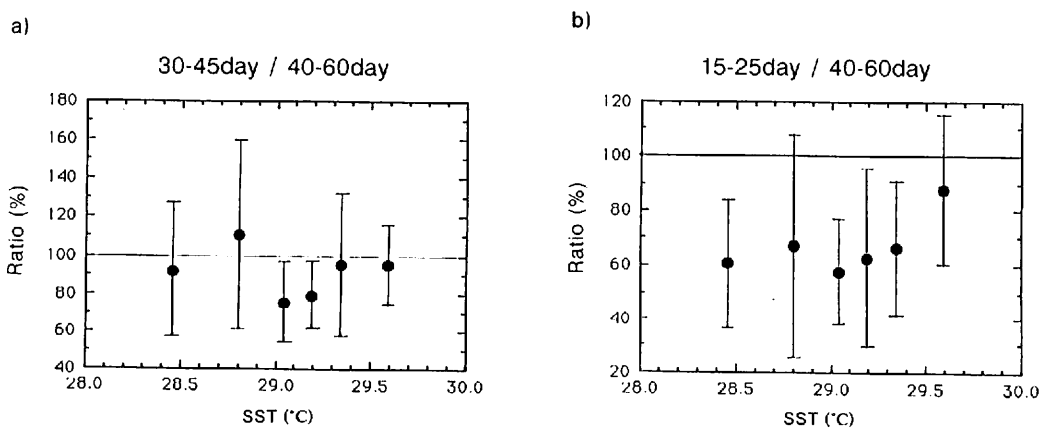

Fig.4.13 (a) Ratio of integrated power of OLR for the 30–45 day period to that for the 40–60 day period in Regions from A to E and during the Northern summer. (b) Ratio of power integrated from 15–25 days to that from 40–60 days.

One of the most crucial questions in this section is why the 30–60 day oscillation is suppressed once the SST is beyond a critical value of about 29.5℃, which shall be termed the *upper threshold.* Figure 4.14 shows the contributions of the SST to tropical convection in regions A to E during the Northern Hemisphere summer. It is found that the OLR diminishes as the SST increases, up to about 29.3℃. This implies that over the equatorial western Pacific, the SST primarily governs large-scale convection with a seasonal time scale even though the SST is above a *lower threshold* value of about 28℃. As large scale convection is active over a warm ocean, the 40–60 day fluctuation is also enhanced as shown in Fig. 4.12. Once the SST exceeds 29.5℃, tropical convection tends to weaken compared with maximum growth, a tendency that is similar to the dependence of the 40–60 day fluctuation on the SST. However, it cannot be easily concluded from the above results that, beyond the upper threshold, convective activity is actually weak and as a consequence the 40–60 day fluctuation is suppressed. This is because the OLR values are still rather low (about 225 Wm^{-2}), even when the SST is above the upper threshold while the integrated power for 40–60 day fluctuation indicates a minimun value of all power spectra. The above problem will further be discussed in later sections.

Next, the fact that a much larger power reduction is found beyond the upper threshold SST of 29.5℃ is verified, through examination of the 10-day mean SST data. First, the 10-day mean SST for the Northern Hemisphere summer of each year is averaged over the western Pacific region (0°–10°N, 130–160°E). Then histograms of SST are constructed in which the bar represents the number of individuals belonging to each class, as seen in Fig. 4.15. For example, the class intervals are chosen as 28.45–28.55, 28.55–28.65, *etc.* The SST fluctuates most frequently in the range from 29.1° to 29.4℃ during May–October 1979 when the 30–60 day oscillation is prominent (see Fig. 4.6). Although the year 1979 is not a typical case, this tendency also appears in several other years. It is clearly seen, on the other hand, that the SST is almost always above 29.5℃ during the northern summer of 1981, when the 30–60 day oscillation is not very pronounced over the equatorial western Pacific.

Here the *threshold index* is simply defined as the ratio of the period when the 10-day mean SST is always above 29.5℃, to the total period from May through October. Using this index the dependence of 30–60 day oscillation on the SST can be investigated in a different manner, as seen in Fig. 4.16. The diagram shows the relationships between the threshold index and the integrated power spectra of OLR for the 40–60 day and the 30–45 day period ranges. For this purpose, the power spectra are averaged over the

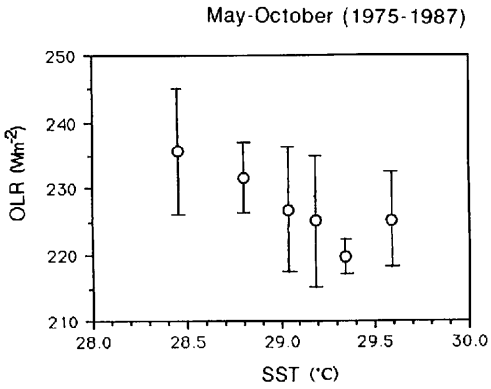

Fig.4.14 Dependence of tropical large-scale convection on SST in Regions A to E during Northern summer.

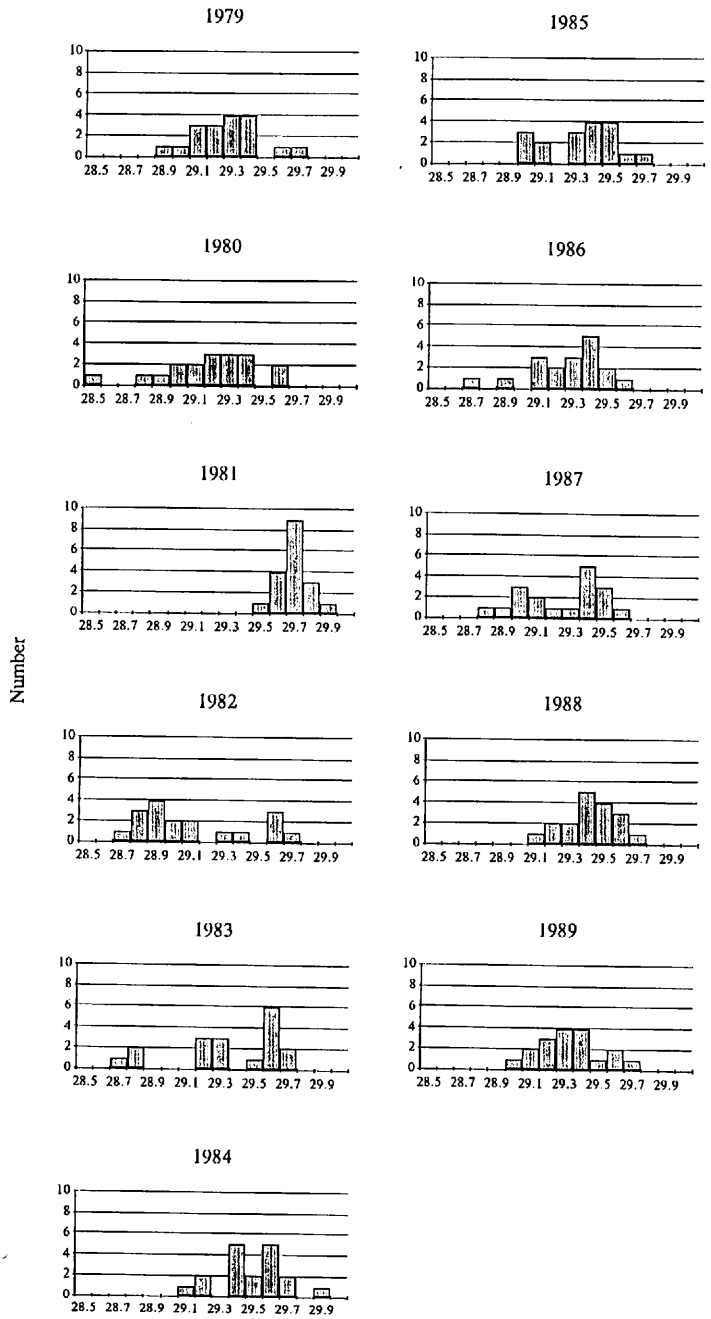

Fig.4.15 Histograms of the 10-day mean SST, which is averaged over the tropical western Pacific region (0°–10°N, 130–160°E), for the Northern summer of each year. The bar is the number of individuals belonging to each class and the class intervals are chosen as 28.45–28.55, 28.55–28.65, *etc.*

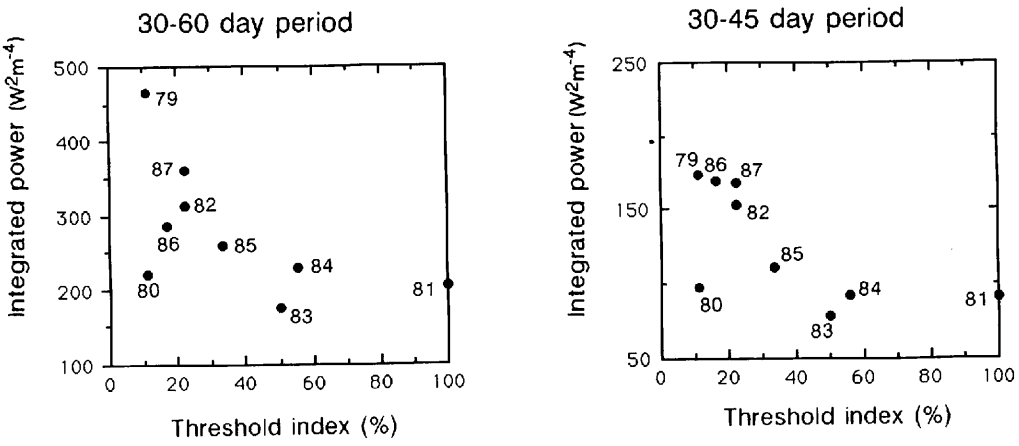

Fig.4.16 Relationships between the threshold index and integrated power spectra of OLR for the 40–60 day and the 30–45 day period ranges, power spectra which are averaged over the western Pacific sector (0°–10°N,130–160°E). The vertical axis is the sum of integrated powers for two period ranges in left panel and integrated powers for 30–45 day period in right panel.

western Pacific sector (0°–10°N 130–160°E). The diagram describes the characteristic that a large reduction in power occurs when the total SST is too high. The left panel, in which the vertical axis is the integrated power spectra for the 30–60 day period range, shows that the power is obviously small in 1981, 1983 and 1984 when the threshold index exceeds around 40 to 50%. This tendency is also indicated for the 30–45 day fluctuation (right panel).

Figure 4.17 shows the proportion of integrated power for the high-frequency fluctuation (15–25 day period) to that for the low-frequency fluctuation (30–60 day period). It is seen that up to 30–40%, the high-frequency fluctuation is relatively emphasized under a high threshold index.

4.5 Coupling between the SST and tropical convection

In the previous section, it was found that the equatorial western Pacific SST has a substantial influence on the development of the 30–60 day disturbances, even when the SST is above a threshold value of around 28°–28.5℃, which suggests that some air–sea feedback systems should be considered for the 30–60 day oscillation. In this section, to explore possible air–sea interactions on intraseasonal time scales, lag-relationships between the SST and large-scale convection are investigated using 10-day mean data.

A strong air–sea coupling on an intraseasonal time scale appears to require the existence of *oceanic* intraseasonal variations. Intraseasonal variations appearing in the tropical SST, sea level or current velocity have recently been examined by Mysak and Mertz (1984), Enfield and Lukas (1984), Spillane *et al.* (1987), Schott *et al.* (1988), Kutsuwada (1988), Krishnamurti *et al.* (1988), among others. Figure 4.18 shows time–longitude cross-sections of SST anomalies over the latitudinal band between the equator and 10°N for the intraseasonal component which was obtained as departures from the smoothed data using a 90-day weighted running mean. It is seen that, from June to October 1979, the amplitudes of the intraseasonal component are large in the region between 130° and 160°E. Large SST anomalies on the intraseasonal time scale have spatial scales of 1000–2000 km, which are equivalent to the scale of a so-called *super cluster*. Hence, it is concluded that the intraseasonal variation of the SST is closely associated with large-

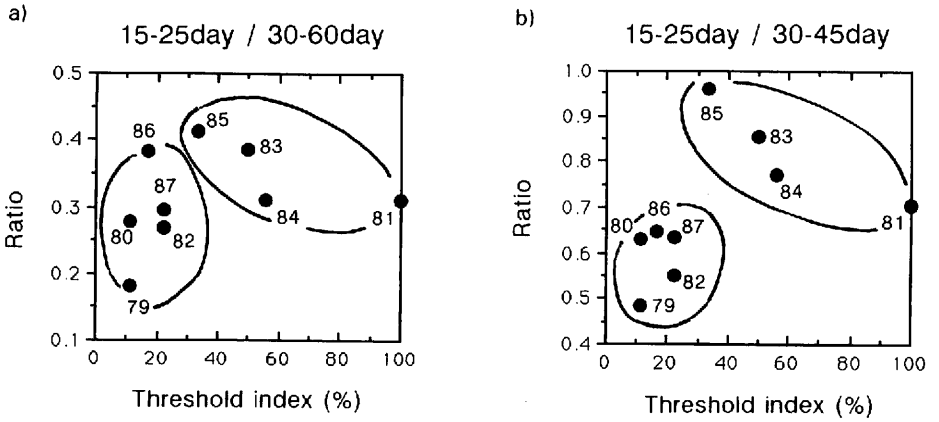

Fig.4.17 (a) Ratio of integrated power of OLR for high frequency fluctuation (15–25 day period) to that for low frequency fluctuation (30–60 day period). Note that the horizontal axis is threshold index.
(b) Ratio of power integrated from 15–25 days to that from 30–45 days.

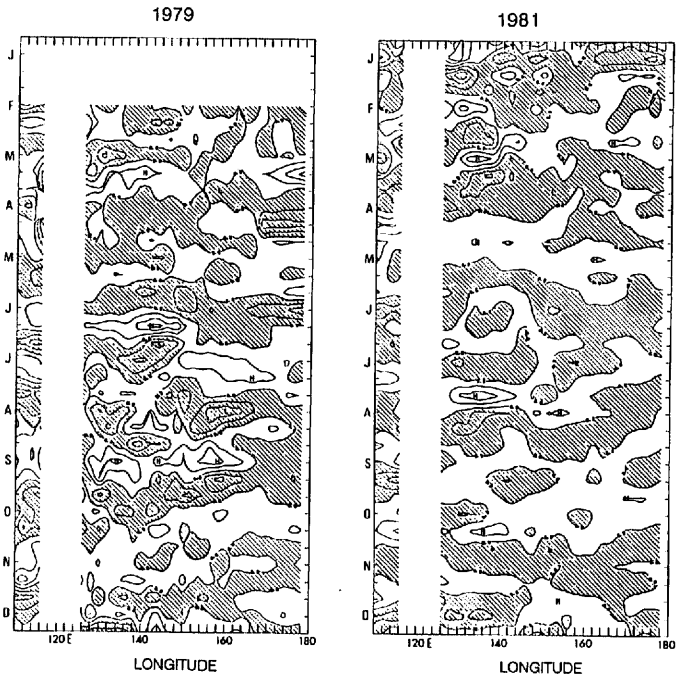

Fig.4.18 Time–longitude cross section of SST anomalies at a latitudinal band between equator and 10°N for the intraseasonal component in 1979 and 1981. Contour interval is 0.2℃ and negative values are shaded.

scale rather than local-scale air-sea interactions. In contrast, as shown in the right panel, distinct SST anomalies on the intraseasonal time scale are not found during 1981, when the SST is very high and the atmospheric 30–60 day oscillation is no prominent over the tropical western Pacific. These results suggest

that the intraseasonal variations of SST are strongly related to those of tropical large-scale convection.

Table 4.1 lists the lag-correlation between the 10-day mean SST and OLR averaged over each region shown in Fig. 4.11. To emphasize the relationships for the intraseasonal time scale, the SST and OLR anomalies are obtained as departures from the smoothed data using a 70-day running mean. The data used are for the period from May through October during the 6 years from 1979 through 1984. In examining the 30-60 day oscillation, the lags are taken from -3 to +3 (one lag is equivalent to 10 days). Positive lag implies that the variation of the SST precedes that of the OLR. The SSTs averaged from May through October over the 6 years are equal to or greater than 29.0°C in all the designated regions. In particular, in Regions A, B, and C where the SST is particularly high, significant correlation coefficients at the 1.0% significance level are found. Significant negative correlations are found at a lag of +1 or +2 in these three regions with the correlation coefficient reaching a value of -0.43 at a lag of +2 in Region C. Significant positive correlations, on the other hand, are found at a lag of -1 in Regions B and C. However, no significant correlations are found for any lag in Regions D and E.

These results show that the SST over the equatorial western Pacific is highly correlated with convective activity, having a phase difference of 10-20 days. Very recently, Murakami (1988) investigated the filtered anomalies of the SST and OLR for the period band of 30-60 days and obtained similar results. That is, there exists a phase difference of 10-15 days between the SST and OLR.

The 30-60 day oscillation exhibits an eastward propagation over the tropical ocean. Therefore, it is necessary to examine the spatial patterns of the lag-correlation between the OLR and SST in order to investigate the air-sea coupling from a spatial viewpoint. Figure 4.19 shows the distributions of lag-correlation coefficients between the tropical OLR anomalies from the Indian Ocean through the central Pacific and the SST in a key region (0°-10°N, 130-160°E), where significant correlations were detected. Weak positive OLR anomalies cover the key region and extend to the central Pacific at lags of -2 and -1. On the other hand, negative anomalies are located in the region from the Indian Ocean to the maritime continent and progress eastward from negative through positive lags. At a lag of +2 (20 days), significant negative anomalies extend into the equatorial western Pacific. Therefore, the SST in the equatorial western Pacific

Table 4.1 Lag-correlation between the 10-day mean SST and OLR over five regions (from A to E, see Fig.4.11) in the western tropical Pacific (0°-10°N, 130°E-180°). Positive lag denotes that the variation in the SST precedes that of the OLR, Significant correlation coefficients at the 99.0% confidence level are indicated by asterisks. The SST averaged from May through October in each region is also shown.

LAG	A	B	C	D	E
−3	0.22	−0.12	0.03	0.06	−0.12
−2	0.21	0.12	−0.02	−0.17	−0.15
−1	0.08	0.27*	0.36*	0.06	0.13
0	0.00	0.25	0.11	0.13	0.09
1	−0.29*	−0.22	−0.20	0.02	0.02
2	−0.08	−0.31*	−0.43*	−0.19	−0.10
3	−0.02	−0.14	−0.06	0.02	−0.01
MEAN SST	29.2	29.4	29.4	29.1	29.0

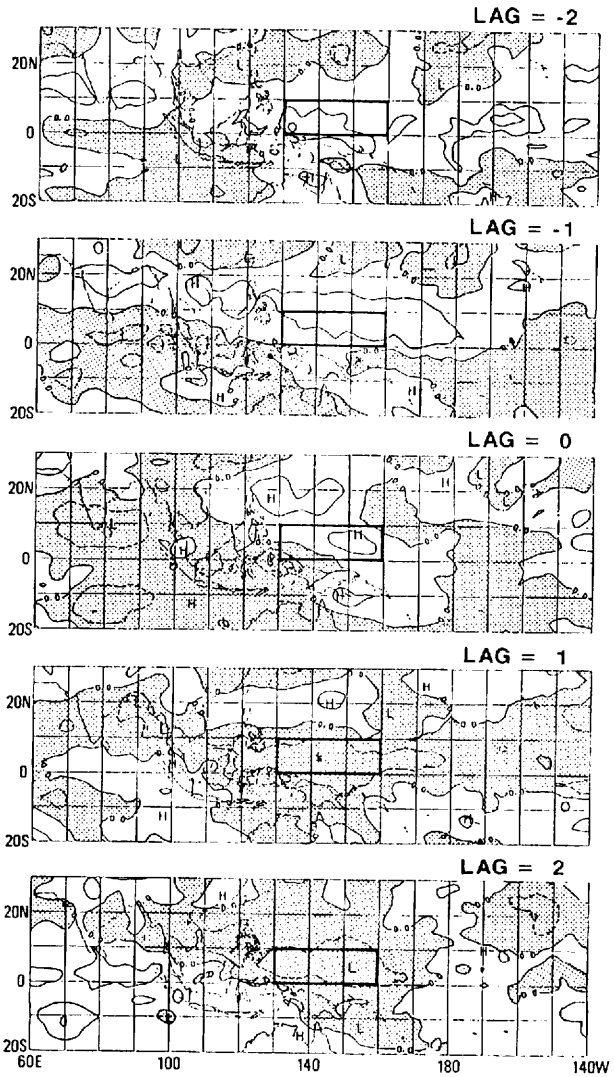

Fig.4.19 Lag-correlation patterns between the OLR anomalies in tropical regions and SST anomalies in the key region (0°–10°N ,130–160°E) shown by the rectangle. Positive lag implies that the variation of SST precedes that of the OLR. The contour interval is 0.2 and negative values are shaded (after Kawamura, 1988b).

and the eastward-propagating disturbance interact with an intraseasonal time scale. The above results also show that the SSTs east of the eastward-propagating 30–60 day mode disturbances are above normal.

Figure 4.20 shows the time series of 10-day mean SST and HCC averaged over the key region for the northern summer (May–October) during the 8-year period from 1979 to 1986. In 1979 and 1986 the SST was between 29° and 29.5°C from May to October and fluctuated out of phase with the HCC. Except for 1981 and 1982, it can be seen that the SST is approximately out of phase with the HCC. In the 1981 case.

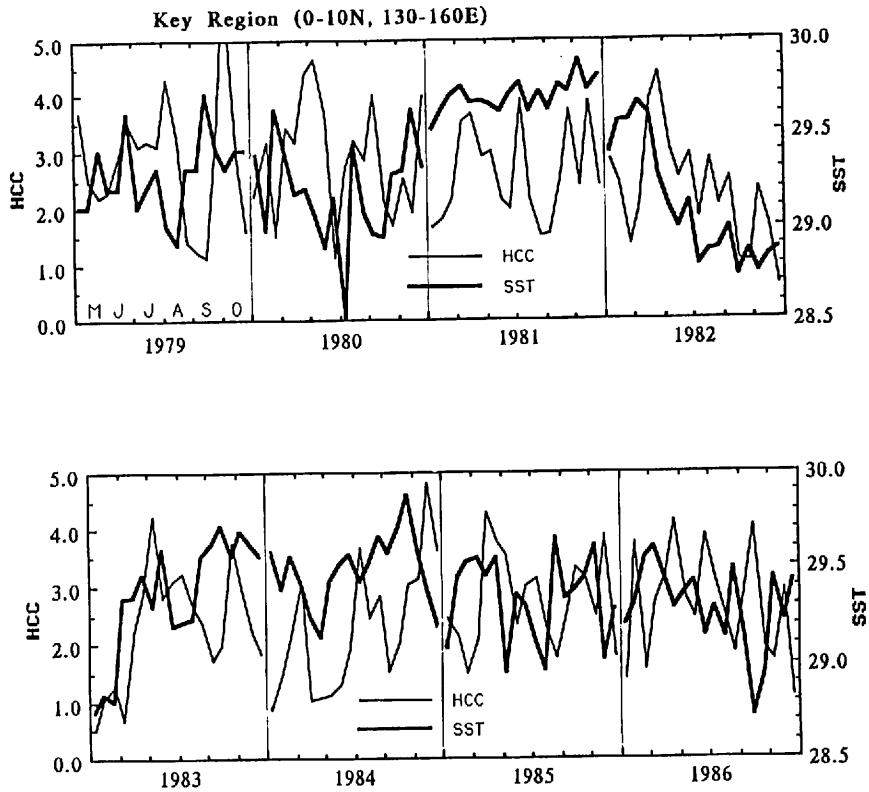

Fig.4.20 Time series of the 10-day mean SST (thick line) and HCC (thin line) averaged over the key region (0°-10N, 130-160°E) during the Northern summer (May-October) during 8-year period from 1979 to 1986.

as mentioned in previous sections, the equatorial western Pasific SST is very warm and always above 29.5℃, while during 1982 the SST is often less than 29℃ although it is greater than 29℃ from May to June. Moreover, during the northern winter when the SST is below 29℃, the HCC and SST do not fluctuate coherently with an intraseasonal time scale (not shown). As shown in Table 4.1, significant correlations between the SST and OLR were not observed for any lag in Regions D and E, where the mean SSTs are around 29℃. It is concluded, therefore, that on the intraseasonal time scale equatorial western Pacific SST tends to couple with tropical large-scale convection during the period when the SST value is around 29°to 29.5℃.

4.6 Possible air-sea feedback on the intraseasonal time scale

The following results were obtained in the previous section:

1) In the warm pool region of the western Pacific, the SST primarily controls large-scale convection with a seasonal time scale even when the SST is beyond a threshold value of 28°-28.5℃. Convection is the deepest when the underlying SST value is about 29.3℃.

2) The growth of the atmospheric 30-60 day oscillation is affected by SSTs above 28°-28.5℃ and the oscillation is prominent when the SST is around 29.3℃. Once the SST exceeds the upper threshold value of about 29.5℃, the 30-60 day oscillation is dramatically damped over the equatorial western Pacific, although large-scale convection is still rather active. The high frequency fluctuation (15-25 day period)

becomes, as a result, more dominant under high SST conditions.

3) When the tropical western Pacific SST is in the range from 29° to 29.5℃, the SST and large-scale convection fluctuate coherently on the intraseasonal time scale with the phase difference between the two being 10–20 days.

At this point, it is pertinent to ask what air-sea feedback system can explain the above results. Several possible air-sea feedback mechanisms on the intraseasonal time scale will be discussed in this section.

Two types of feedback mechanisms that exist in the air-sea coupled system are the negative and positive feedback mechanisms. A well-known negative feedback of convection is the cloud-SST feedback. That is, clouds diminish the incoming shortwave radiation, which creates active turbulent mixing in the ocean mixed layer, and thereby decreases the SST which in turn reduces evaporation, leading to diminished clouds. This feedback has a damping effect for the growth of SST anomalies. However, negative feedback cannot create an unstable air-sea coupled mode which is necessary for the occurrence of ENSO. The unstable air-sea coupled mode requires a positive feedback mechanism.

Philander *et al.* (1984) showed that if the ocean mixed layer deepens in the wind convergence region with the SST being proportional to the depth of the mixed layer, positive SST anomalies occur in the region. The destabilization of the oceanic Kelvin wave excites an eastward-propagating unstable air-sea coupled mode. This process has a positive feedback since positive SST anomalies formed by wind convergence in the lower troposphere in turn increase the wind convergence.

On the other hand, a positive feedback which does not require wave dynamics was presented by Chu and Garwood (1990) and others. Precipitation results in low-salinity layers in the upper ocean; the decrease in salinity increases the stability of the upper ocean, effectively reducing the deepening of the ocean mixed layer. Under such conditions an increase in the SST occurs easily with concentrated downward net radiation flux and heat flux across the ocean surface. The resulting increase in evaporation leads to an increase in clouds. Accordingly to Lukas (1988), strong precipitation in the warm pool region forms a low salinity layer (a *barrier layer*) where the SST is not usually influenced by oceanic Kelvin and Rossby waves.

Although several air-sea feedback mechanisms can be considered, it is still uncertain which air-sea feedback system is essential or effective for each time and spatial scale. However, some observational results derived from the previous section suggest that both positive and negative feedback systems, which respectively act as the growing and damping effects on the SST anomaly, dominate when the mean SST is

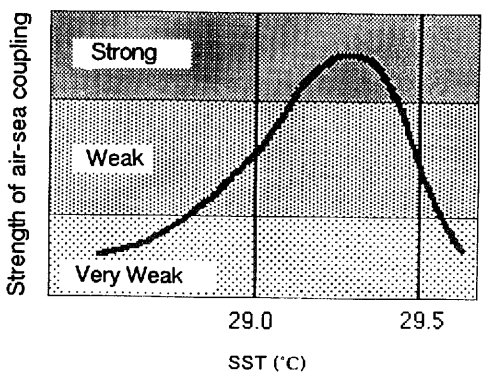

Fig.4.21 Schematic diagram representing the dependence of the strength of air-sea coupling in the intraseasonal time scale on tropical western Pacific SST.

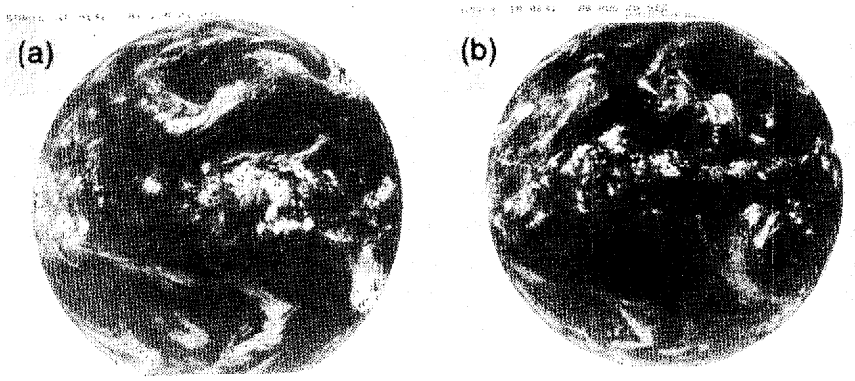

Fig.4.22 (a) Snapshot of infrared image from GMS for June 22, 1987.
(b) As in Fig.4.22 (a), but for August 25, 1988.

around 29° to 29.5℃. This implies the presence of a strong air-sea coupling on the intraseasonal time scale. When the equatorial western Pasific SST is above the lower threshold (28°-28.5℃), large-scale convection can grow rapidly through the CISK mechanism, if moisture convergence occurs in this region. However, the 30-60 day oscillation especially in lower-frequency range is, to some extent, dependent on the SST even though the mean SST is beyond 28.5℃ and is prominent for SST values of around 29.3℃. It is concluded that the strong air-sea coupling on the intraseasonal time scale occurs at this time, as illustrated in Fig. 4.21. Once the SST is beyond the upper threshold value of about 29.5℃, the 30-60 day oscillation is dramatically damped, while tropical large-scale convection is still rather active. At this point the air-sea coupling on the intraseasonal time sclae relaxes and high-frequency fluctuations become relatively dominant. Hence, it is concluded from the above discussion that over the warm pool region of the western Pacific the 30-60 day oscillation is presumably modified by strong air-sea interaction on the intraseasonal time scale.

One of the reasons why the 30-60 day oscillation is decayed under too high SST condition appears to be the weakness of the air-sea coupling on this time scale. The following discussion is speculation.

It is naturally expected that the air-sea interaction on the so-called super-cluster scale is considerably different from that of the cloud-cluster scale. The left panel of Fig. 4.22 shows an infrared image from the GMS for June 22, 1987, when the 30-60 day oscillation was active over the equatorial western Pasific. It is clearly seen that a super cluster exists over the equatorial western Pacific. The super cluster produces an increase of mixed-layer entrainment in the underlying upper ocean, decreasing the SST as a result, although there is a necessary condition that the mixed layer is not extremely deep. The 30-60 day disturbances with the accompanying supper clusters propagate eastward over the warm pool region, resulting in the warm ocean condition of about 29.5℃ being hardly persistent over several months. On the other hand, the right panel of this diagram shows an infrared image for August 25, 1988. No notable super clusters are seen over the western Pacific and normal cloud clusters are widely distributed in the region. Such cloud clusters are unable to produce large-scale negative SST anomalies and further difficulty occurs when warm water is widely accumulated in the western Pacific. Consequently, tropical western Pacific SSTs above 29.5℃ persist over several months, and no significant intraseasonal variations of SST are seen.

In this chapter, possible SST effects have been discussed as a background in which the 30-60 day oscillation develops over the tropical ocean. As a result, it was shown that the air-sea coupling on the in-

traseasonal time scale can not be disregarded. Although the 30–60 day disturbances significantly propagate eastward, no eastward-propagating air–sea feedback systems in the warm pool region of the western Pacific were discussed. It is also exepected that the air–sea coupling on the intraseasonal time scale is forced to change when warm water is piled up in the western Pacific. Therefore, the air–sea couplings on interannual time scales should also be considered. The above problems will be examined in the next chapter.

CHAPTER V

AIR–SEA COUPLED MODES WITH INTERANNUAL AND INTRASEASONAL TIME SCALES

5.1 Data

Daily 850mb zonal wind (u) data on a 2.5° latitude by 2.5° longitude grid were derived from global analyses by the European Center for Medium Range Weather Forecasts (ECMWF). The data assimilation system of the ECMWF global analyses is described in detail by Hollingsworth *et al.* (1986). Although the major changes in the data assimilation system have had the greatest impact on the divergent wind component and related vertical motion fields, along with the moisture fields (Trenberth and Olson, 1988), the zonal wind fields in the lower troposphere have been shown to be more reliable than the above quantities.

The SST and HCC data are also used, whose explanations have been given in Section 4.1. The data during the period from January 1980 to December 1986 are analyzed when all the data were available.

5.2 Analysis procedures

Before investigating how the variables SST, HCC, and 850mb u fluctuate with intraseasonal and interannual time scales, the HCC and 850mb u data were first calculated 10-day mean values. The purpose of this was to compare them with the SST fluctuations since the SST data having a shorter time scale than 10 days are not currently available. Even if utilization were made of such data, there exist a number of missing observations; also, the analyzed region is limited to within narrow bounds. Second, the intraseasonal component and the interannual component must be extracted. The original n-th 10-day mean data for year i of a variable is denoted by $[Xn]i$ ($n=1,36$) with the anomaly value X^* from the long-term mean being computed by

$$X^*=[Xn]i-\overline{Xn}. \tag{5.1}$$

where $\overline{Xn}$ represents the 7-year (1980–1986) mean at the n-th data. The interannual component X_L is defined as a 90-day weighted moving average as follows:

$$X_L=\sum_{k=-4}^{4} w_k X^*_{m+k}. \tag{5.2}$$

where the filtering function w_k having $\sigma=T/6$ (T is equal to 90 days) is given as

$$w_k=(2\pi\sigma^2)^{-1/2} \exp(-k^2/2\sigma^2). \tag{5.3}$$

Next, the intraseasonal component is computed by

$$X_S=X^*-X_L. \tag{5.4}$$

Thus, we can obtain the interannual componet X_L and the intraseasonal component X_S of each variable SST, HCC and 850mb u. Based on the original 10-day mean data, X_S represents the 30–60 day oscillation better than the other high-frequency oscillations.

Phase relationships among the three variables are statistically examined for each time scale in several regions of the tropical western Pacific, using the CEOF analysis. The complex time series $X(j,t)$ is obtained from a Hilbert transform of $x(j,t)$, the normalized time series of each variable j. $X(j,t)$ is expanded into a sum of EOFs as follows.

$$X(j,t)=\sum_{m=1}^{3} Fmt\ Bm^*(j), \tag{5.5}$$

where the asterisk implies a complex conjugation, $Bm(j)$ represents the complex eigenvector of the j-th variable for the m-th mode, and Fmt is the complex coefficient for $Bm(j)$.

Considering only three variables SST, HCC, and 850mb u, the eigenvalue problem of the 3×3 complex correlation matrix (Hermite matrix) is solved. The amplitudes $A(j)$ and phases $P(j)$ of the first CEOF modes of the intraseasonal and interannual time scales in each region are also computed. $A(j)$ and $P(j)$ can be obtained as

$$A(j)=[Bm(j)\ Bm^*(j)]^{1/2}, \tag{5.6}$$

and

$$P(j)=\tan^{-1}[\mathrm{Im}\ Bm(j)\ /\ \mathrm{Re}\ Bm(j)]. \tag{5.7}$$

In this study only the first CEOF modes are considered with the first modes for the intraseasonal and interannual time scales being called the intraseasonal mode and the interannual mode, respectively. Also, in order to investigate the amplitude modulations of these modes the temporal amplitude function AMt is defined as

$$AMt=[Ft\ Ft^*]^{1/2}. \tag{5.8}$$

5.3 Phase relationships among the SST, high-cloud cover and zonal wind at the 850mb level

The climatological mean HCC field over the western Pacific during the period from 1980 to 1986 has previously been shown in Fig. 4.11. To examine the phase relationships of air-sea coupling, the equatorial western Pacific sector where convective activity is strong is divided into five regions (10° latitude by 10° longitude), as shown in Fig. 4.11. To begin with, attention will be focused on a key region (0°-10°N, 130-160°E), which includes Regions A, B and C, where lag-correlations between the SST and OLR on the intraseasonal time scale are especially significant (see Table 4.1).

Figure 5.1 shows the time series of HCC, SST, and 850mb u for the two time scales in the key region the 7-year period 1980-1986. For the interannual component of HCC, signficant negative anomalies are observed during the period from the fall[1] of 1982 to the spring of 1983, corresponding to the 1982/83 ENSO, whereas marked positive anomalies are not found. The amplitudes of the intraseasonal component tend to be large during the years 1980 and 1984. Positive SST anmalies for the interannual component are apparent during the period from the summer of 1981 to the spring of 1982 and reach a maximum value of +0.4℃. After the summer of 1982, the SST decreases rapidly and negative anomalies exist until the spring of 1983. During the fall of 1983 to the summer of 1984, the SST tends to be high. The amplitudes of

1 The seasons discussed here are with reference to the Northen Hemisphere.

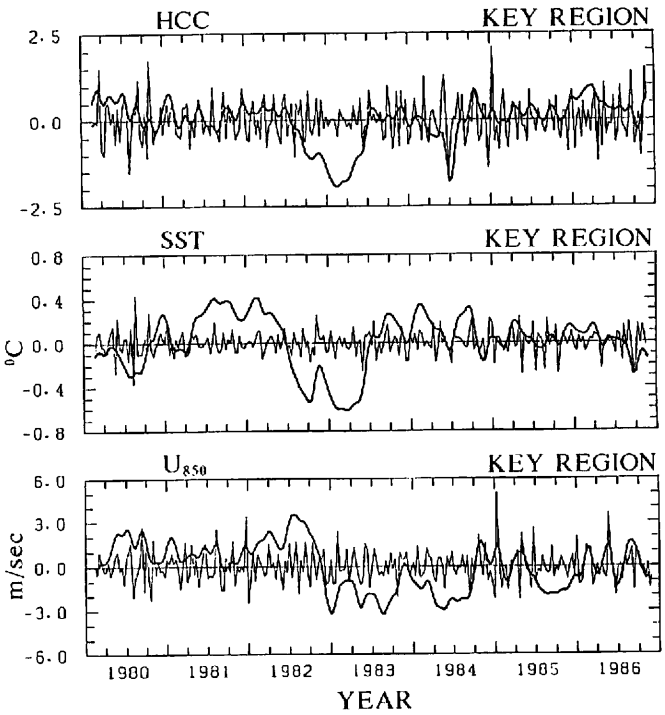

Fig.5.1 Time series of HCC, SST and 850mb u in the key region for the intraseasonal component (thin line) and the interannual component (thick line).

the intraseasonal component are largest during 1980, but small during the summer of 1981 to the spring of 1982 when the SST is anomalously high. Positive (westerly) anomalies of 850mb u, on the other hand, are persistent on the interannual time scale during the 3-year period (1980-1982) and reach a maximum value of 3.5 m/s around July 1982. After this period anomalous easterly winds are enhanced and presistent for about two years. The intraseasonal component is active druing the periods of 1980 to 1981, the winter of 1984/85, and 1986.

It is found from the above results that, for the interannual time scale, the maximum and minimum phases of a variable do not coincide with those of other variables being associated with remarkable phase differences among the three variables. For the intraseasonal component, the amplitudes of all the three variables are large during the year 1980, but during ohter periods it is not necessarily observed that the amplitudes of all the variables are enhanced for the same period.

Although the key region has been noted, the other regions of the tropical western Pacific need further examination. Therefore, time series of the three variables (SST, HCC and 850mb u) for the two time scales in Regions A and E are also shown in Figs.5.2 and 5.3, respectively. Comparing Fig. 5.2 with Fig. 5.3, it can be seen that the amplitude of the intraseasonal component in Region A is greater than that in Region E. It is also seen that the intraseasonal component in Region A is active during the 1980 year period, whereas that in Region E is active during other periods. For example, in Region E strong westerly winds on the intraseasonal time scale occur about November 1982 and nearly during the same period westerly anomalis of the interannual component are rapidly dissipated. In contrast, the amplitude of the interannual component in Region E tends to be greater than that in Region A. In Region E, high SST anomalies and westerly anomalies persist during the period from 1980 to 1982 whereas, after 1983, low

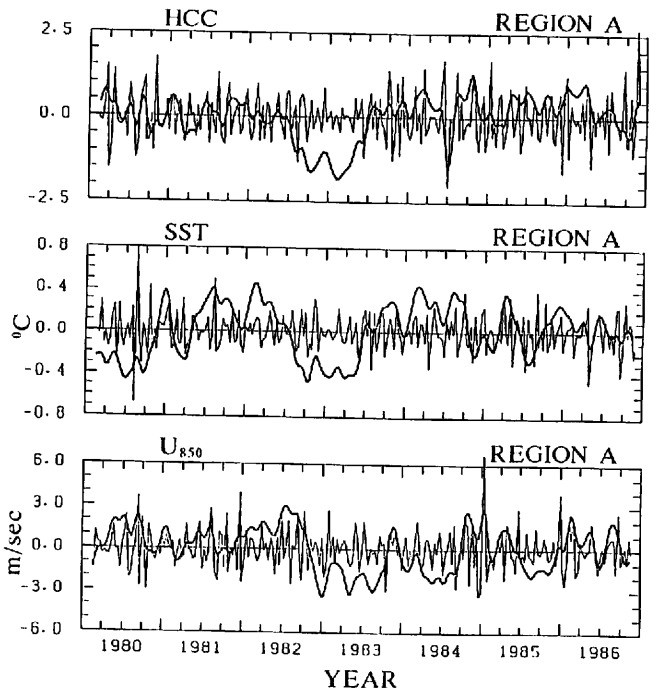

Fig.5.2 As in Fig.5.1, but for Region A.

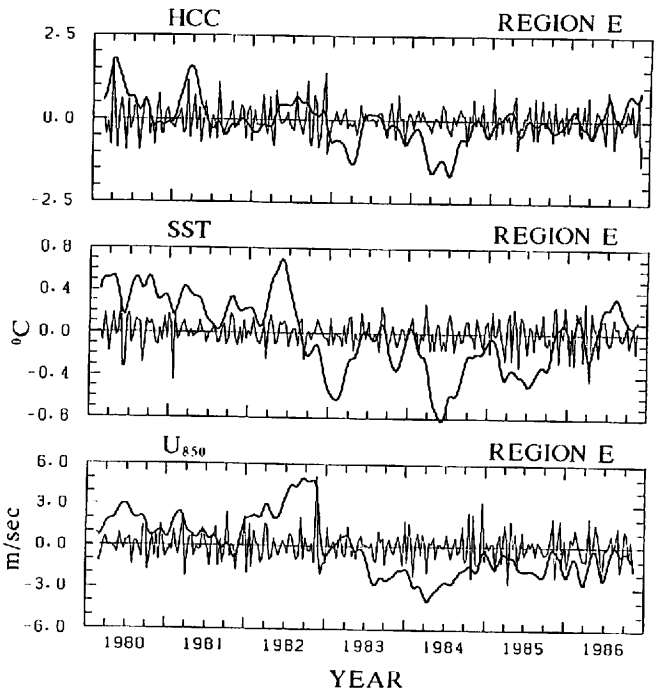

Fig.5.3 As in Fig.5.1, but for Region E.

SST anomalies and easterly anomalies are dominant. Thus, it can be clearly seen that, in Region A, intraseasonal variations prevail compared with the interannual variations while, in Region E, the interannual variations are prominent. This implies that the region where the two components are dominant differ from each other. Furthermore, it is also expected that phase relationships among the three variables vary with region and time scale. The phase relationships among the three variables in Region A, E, and the key region should be statistically examined.

Figure 5.4 shows the amplitudes *A(j)* and phases *P(j)* of the first CEOF modes for the intraseasonal and interannual time scales in each region. The intraseasonal mode has a similar tendency in all regions. The ratios of the explained variance to the total variance in Region A, key region, and Region E are 50.7%, 51.5%, and 45.2%, respectively. In this mode the HCC is almost in phase with the 850mb *u*, that is, the maximun of HCC is in accord with that of the westerly wind at 850mb, while the SST leads HCC by around 140°–170°. Noting the key region where the variance is largest of all regions, it can be seen that the amplitude of the SST is somewhat smaller than that of the HCC or 850mb *u* and the phase difference between the SST and HCC is about 140°. This means that, on the intraseasonal time scale, the HCC (or westerly wind at 850mb) couples with the SST with a phase shift of 10–20 days. The above result is consistent with those of previous observational studies (see, Kawamura, 1988b; Murakami, 1988).

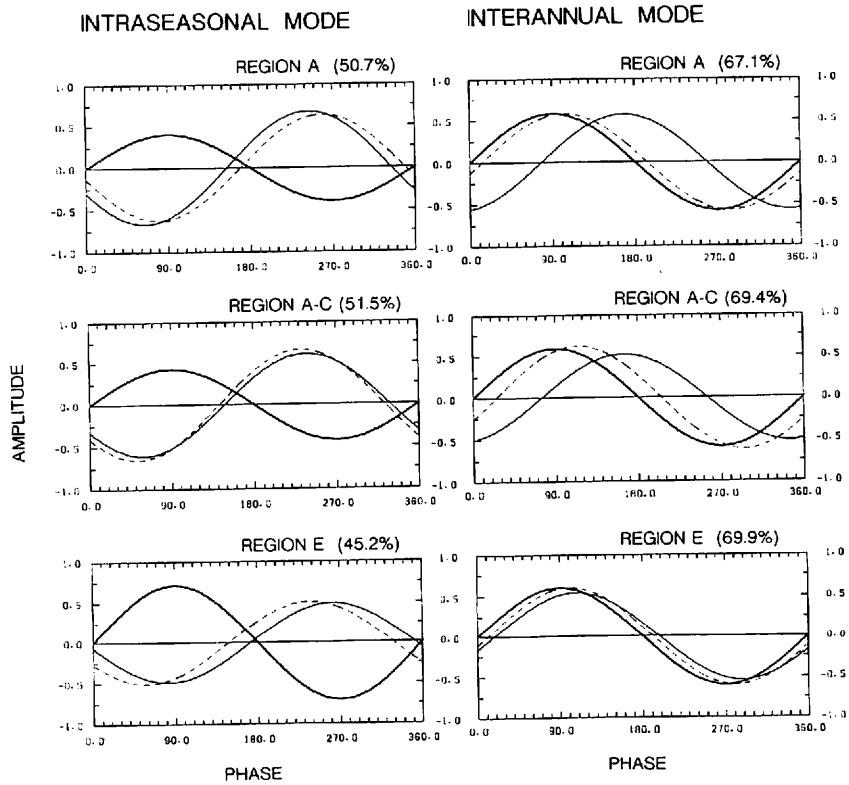

Fig.5.4 The amplitudes and phases (degrees) of SST, HCC and zonal wind at 850mb on the intraseasonal and the interannual modes. The SST, HCC and 850mb *u* are denoted by thick, dashed and thin lines, respectively. Note that the ratio of the explained variance to the total variance, expressed as percentages, is also shown for each region.

On the other hand, it should be noted that the interannual mode has a tendency to depend on the region. The ratios of the explained variance to the total variance in Region A, the key region, and Region E are 67.1%, 69.4%, and 69.9%, respectively. The variances of this mode become large from the western Pacific eastward to the dateline. The amplitude of the SST is almost as large as that of HCC while the SST leads HCC by around 10°–30°. It is further seen that the phase of 850mb u exhibits an obvious shift between Regions A and E, *i.e.*, in Region A the phase lag between SST and 850mb u is about 80°, whereas in Region E the 850mb u lags the SST by only about 20°. Since the interannual mode includes the time scales of the ENSO and QBO, it is inferred that when the SST over the western Pacific is anomalously high, the HCC reaches its maximum about 1–3 months later. The maximum of westerlies at 850mb lags that of the HCC by 3–7 months in the key region and by less than 1 month for region E.

5.4 Characteristics of the interannual and intraseasonal modes

Although the above results account for the phase relationships of air–sea couplings on the two time scales, it is still uncertain how the amplitude modulations of these modes evolve with time. Figure 5.5 demonstrates the temporal amplitude function *AMt* of each mode with respect to each region. It is considered from this figure that both interannual modes in Region A and the key region are basically the same, as also shown in Fig. 5.4. It can be seen that the interannual mode develops in both regions during the period from 1982 to 1983. This period beyond a year is equivalent to the life cycle that occurs with the ENSO phenomenon: genesis, development and decay. This appears to prove that the ENSO is one of the prominent phenomena in air–sea couplings on the interannual time scale. The second maximum peak appears about July–October 1984, but the mode for this period does not develop to any great extent and has a short life of within only half a year. The interannual mode in Region E is somewhat different from those in

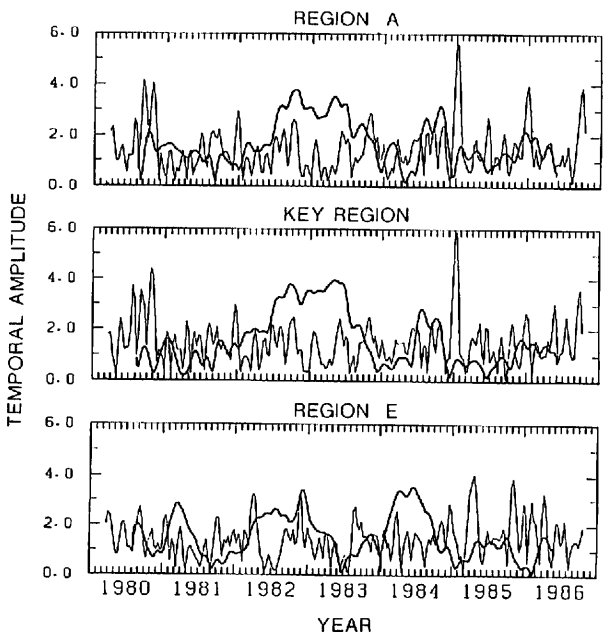

Fig.5.5 The temporal amplitude function of each leading mode in Region A, the key region and Region E. The intraseasonal and interannual modes are denoted by thin and thick lines, respectively.

other regions and appeas to be a frequetly developing mode, as seen in Fig. 5.5.

On the other hand, the *AMt*s of the intraseasonal modes in Region A and the key region are amplified in 1980 and around January 1985. In these regions, *AMt*s tend to be somewhat small during the period from 1982 to 1983 when the interannual mode is prominent. In Region E, periods of extremely dominant *AMt* are not observed.

Next, with the use of origianl data, the characteristics of the air-sea couplings from another viewpoint are demonstrated, although the dominant modes in the two time scales are objectively extracted with the use of the CEOF analysis. Figure 5.6 shows scatter diagrams of the 10-day mean SST and HCC in the key region. Figs. 5.6a and b exhibit the relationships between the SST and HCC during the 7-year period (1980-1986) at lags of 0 and +2, where a positive lag implies that the variation of the SST precedes that of the HCC, where one lag is equivalent to 10 days. At a lag of 0 no linear relationship can be found. It is seen

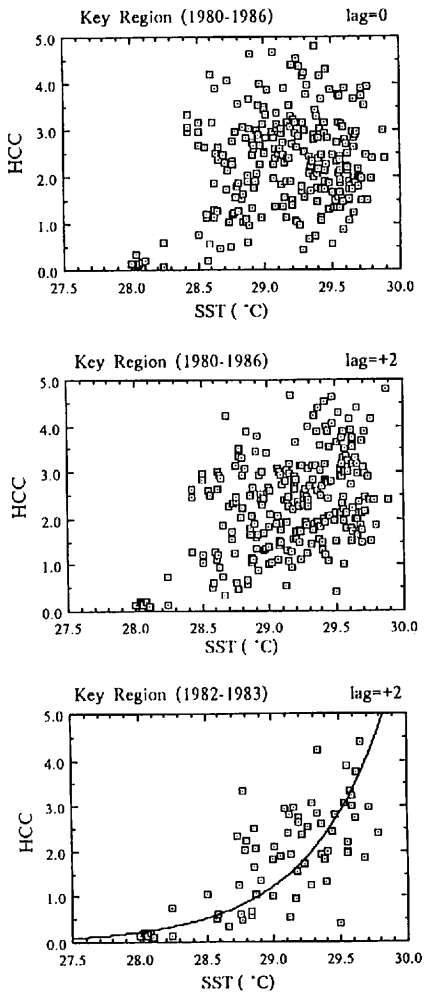

Fig.5.6 Scatter diagrams of 10-day mean SST and HCC in the key region at lags of (a) 0 and (b) +2 during the period from 1980 to 1986, and at a lag of (c) +2 during the 1982-1983 period, involved by a least-squares curve. Positive lag means that the variation in HCC lags that in SST and one lag corresponds to 10 days.

in the key region that the SST is always above 28℃ while the HCC increases rapidly if SST is beyond the threshold value of 28.4℃. Thus, it is likely that the HCC is very nearly independent of SST when the SST is beyond the threshold value. However, at a lag of +2, the HCC depends on the SST to some extent even if the SST is greater than 28.4℃. The phase difference of 20 days between the SST and HCC corresponds with the intraseasonal mode and therefore it means that Fig. 5.6b reveals the relationship between the SST and HCC for a lower-frequency scale, removing the phase difference caused by the intraseasonal oscillation. Although Fig. 5.6c depicts the relationship only during the period from 1982 to 1983 when the interannual mode is dominant, an approximate exponential relationship can be seen for the case when the SST exceeds about 28.5℃. This is consistent with the results that the SST is nearly in phase with the HCC with respect to the interannual mode.

Figure 5.7 indicates relationship between SST and 850mb u in the key region at a lag of +2, where a positive lag implies that the variation of the 850mb u lags that of the SST. In order to see the interannual component, a lag of +2 is taken since the phase lag between the SST and 850mb u is about 150° for the intraseasonal mode. The left panel of this figure is computed from the data during the 7-year period from 1980 to 1986. Characteristic relationships are not apparent, but at least there is no linearity. The right panel is as in Fig. 5.6c except it is for the relationship between the SST and 850mb u. The SST fluctuates around 29.0℃ to 29.5℃ from January to May 1982. During June-October 1982, westerly winds are dominant and simultaneously the SST has a tendency to decrease. This shows that the phase lag between the SST and 850mb u obviously exists on the interannual time scale. In fact, as indicated in Fig. 5.4, the 850mb u lags SST by around 70°-80°. However, in Region E, the SST becomes nearly in phase with the 850mb u. That is, from Fig. 5.8 showing results for region E, it is observed that linear relationships between the two variables are basically found at only lags of 0 and +2. Although the period when westerly winds are prominent corresponds to about July-November 1982, corresponding points for this period fall way off the plotted computed regression line. This implies that the air-sea coupling at the onset phase of the 1982/83 ENSO is minor in Region E. It also appears that this region is not influenced to any great extent by the intraseasonal mode, since the relationship at 0 lag is more linear than that at a lag of +2.

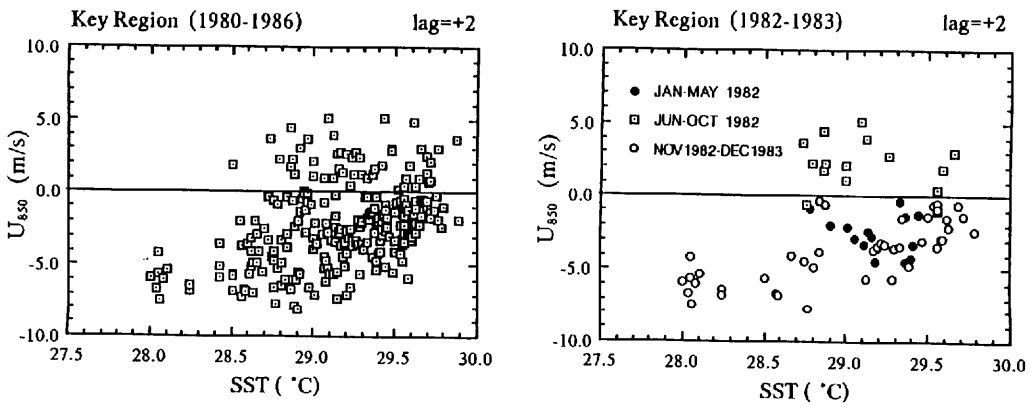

Fig.5.7 Scatter diagrams of 10-day mean SST and 850mb u in the key region at a lag of +2 during (a) 7-year period (1980-1986) and during (b) 2-year period (1982-1983). Positive lag denotes that the variation in SST precedes that in 850mb u.

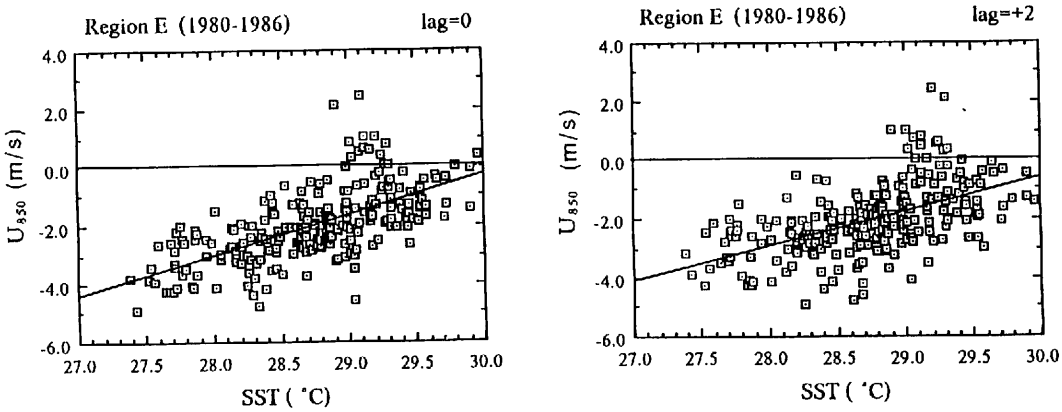

Fig.5.8 Scatter diagrams of 10-day mean SST and 850mb u in Region E during the period from 1980 to 1986 at lags of (a) 0 and (b) +2. Each least-squares line is also shown.

5.5 Multiscale air–sea coupled system

It is found from the above results that remarkable differences exist in the air–sea coupling between the intraseasonal and interannual time scales. The intraseasonal mode reveals similar phase relations over the tropical western Pacific. For this mode the SST is approximately out of phase with the HCC and 850mb u. A schematic diagram of the intraseasonal mode is illustrated in Fig. 5.9a. The area of maximum SST anomaly lies to the east of the center of active convection and thus the SST anomalies tend to be positive in the easterly anomaly area. Since the eastward propagation of the 30–60 day oscillation is generally obvious over the western Pacific, it is inferred that positive SST anomalies are located to the east of the eastward-propagating large-scale disturbance having an intraseasonal time scale. Emanuel (1987) and Neelin *et al.* (1987) suggested that the evaporation-wind feedback mechanism leads to the eastward propagation of the intraseasonal disturbance. The evaporation-SST feedback mechanism may be an important physical process in controlling the growth of a large scale disturbance even if the SST exceeds about 29℃. It is possible that the existence of high SST in the easterly anomaly area favors its further eastward propagation.

The intraseasonal mode is very similar to the advective mode presented by Lau and Shen (1988) with respect to the phase relationship. They claim that the advective mode is caused by the air–sea interaction due to east-west SST advection, and therefore their mode requires an east-west SST gradient. They assumed the tropical Pacific around 140°E-140°W has an east-west SST gradient of 4℃/10,000km. However, the intraseasonal mode defined in this paper exists over the warm pool region where the east-west SST gradient is small. Figure 5.10 shows the time series of the east-west SST gradient over the tropical western Pacific, which is defined as the SST difference between Regions A and E. Here, a positive gradient implies that the SST in Region A is higher than that in Region E. For the periods when the intraseasonal mode is dominant in the key region, negative values are mostly observed in the year 1980. Further, there is almost no gradient around January 1985. Hence, it is inferred that the east-west SST gradient is not a necessary condition for the intraseasonal mode.

The above discussion leads to the conclusion that the qualitative nature of the intraseasonal mode is somewhat contrary to the assumptions required by the advectiv mode and that an observational example of the intraseasonal mode is not always identified with this mode. Therefore, the intraseasonal mode may

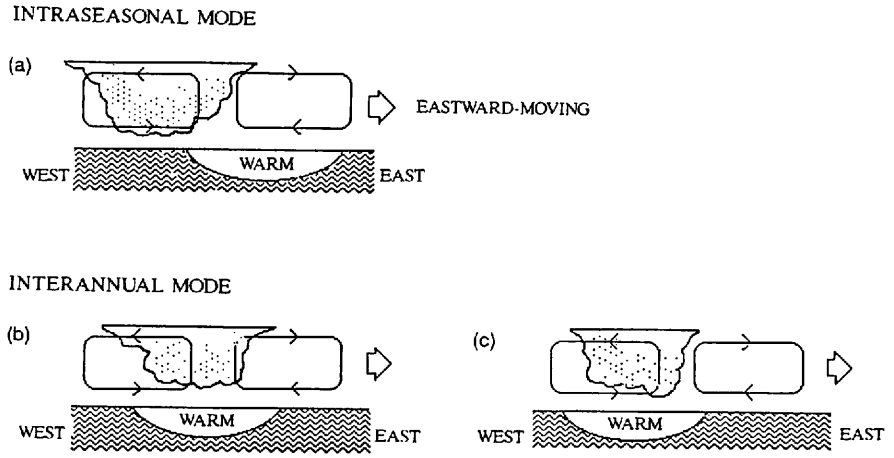

Fig.5.9 Schematic diagrams displaying the phase relationship of air–sea coupling on (a) the intraseasonal mode for the key region and on the interannual mode for (b) the key region and (c) Region E.

require another mechanism other than the east–west SST advection causing the advective mode. Another possible mechanism considered is that the intraseasonal variations of the SST in the warm pool region arise from variations in incoming short-wave radiation and turbulent mixing in the ocean mixed layer, induced by large-scale intraseasonal disturbances. Sui and Lau (1989) report that convective heating maximized above and below the 500mb level excites the fast (20-day) wave and the slow (50-day) wave, respectively. Although their results suggest that fast wave is dominant over the warm pool region of the western Pacific, the observed intraseasoanl oscillations propagate slowly eastward in this region. The intraseasonal variations, which are easily modified by strong air–sea interaction, have spectral peaks in a wide (30 to 60 days) period range. This is because such effects as the reduced incoming solar radiation and active turbulent mixing accompany the large-scale disturbance and result in a decrease of SST.

It is also found that the air–sea coupling on the interannual time scale with longitude over the tropical western Pacific. For the interannual mode, the SST leads HCC by about 20°, but the phase relation of the 850mb u varies from region to region. Figures 5.9b and c schematically demonstrate the essential features of the interannual modes in the key region and Region E, respectively. The ENSO and the QBO modes, which occupy a large part of the interannual mode, are eastward-propagating modes (Arkin *et al.*, 1983; Barnett, 1983; Yasunari, 1985; Meehl, 1987; Gutzler and Harrison, 1987; Kawamura, 1988a). The SST–HCC negative feedback may not be essential to these modes since the SST and HCC tend to be nearly in phase. If only the phase relationships are noted, it is seen that the interannual mode in the key region is similar to the upwelling mode presented by Lau and Shen (1988). It appears that, on the interannual time scale the effect of oceanic upwelling cannot be denied even in the air–sea couplings. In Region E, on the other hand, the SST has a tendency to be high in the westerly anomaly area, being quite contrary to the intraseasonal mode. According to the evaporation–wind feedback mechanism, active evaporation to the east of the center of the large-scale disturbance favors its eastward propagation if the mean wind is easterly. However, since the interannual mode in Region E has the feature of negative SST anomalies to the east of the most convective area, necessary conditions for eastward movement of this mode are not as satisfied as those of the intraseasonal mode. In Region E, a linear relationship exists between the SST and 850mb u,

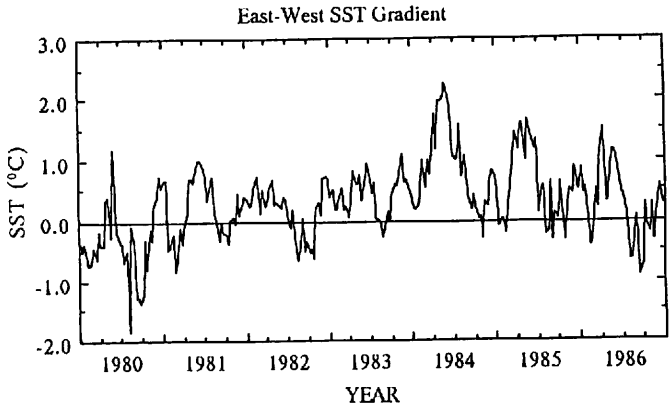

Fig.5.10 Time series east-west SST gradient, which is defined as the SST difference between Regions A to E, in the warm pool region of the western Pacific. Positive SST gradient means that the SST in Region A is higher than in Region E.

as indicated in Fig. 5.8. However, plots of the period from July to November 1982, when westerly winds are dominant, obviously do not fall on a least-squares line. The air-sea coupling during this period is due to the interannual mode defined in the key region, which deveolps and propagates eastward to the central Pacific. The interannual mode for Region E, therefore, should be distinguished from that for the key region. The air-sea coupling over the western pacific, associated with the time evolution of ENSO, is represented by the interannual mode in the key region. It is considered that the mode in Region E rather accounts for the air-sea coupling when large-scale convection is not very active.

In this chapter, the existence of possible interactions between the interannual and the intraseasonal modes of the atmosphere-ocean system could not be confirmed from the viewpoint of amplitude modulation. However, it is found that the strength of the air-sea coupling varies with the years for both time scales. The interannual mode is somewhat amplified during the latter period of 1984. It appears that the air-sea coupled mode during this period would have grown into an ENSO event if some conditions under which it developed were satisfied. Since the variances of the interannual mode are larger than those of the intraseasonal mode, it may be natural that the air-sea coupling as in an ENSO event is stronger than that in the intraseasonal time scale.

The phase relationships of air-sea couplings on two time scales have been statistically examined only over the western Pacific. However, since the analyzed period is rather short from 1980 to 1986, and 10-day mean data were used instead of daily data, detailed discussions are limited. Long-term daily data, especially of SST, need to be accumulated. Further understanding of the air-sea couplings of eastward-propagating modes for the two time scales will be obtained if a similar analysis is applied to the eastern Pacific and Indian Oceans. It is still uncertain why the strengh of air-sea coupling varies from year to year, which will be an important topic of future work.

CHAPTER VI

CONCLUDING REMARKS AND DISCUSSION

This paper addresses the question of large-scale air-sea coupling in the warm pool region of the western Pacific on intraseasonal and interannual time scales. The following results were obtained.

Interannual time scale

The interannual variability of the main thermocline in the equatorial western Pacific along the 137°E longitude line is reflected primarily in the quasi-biennial oscillation (QBO) time scale. The QBO mode of the 700 mb zonal wind, determined by applying a complex EOF (CEOF) analysis, propagates eastward over the tropical Indian and Pacific Oceans with a uniform phase speed. On the other hand, the QBO mode of the SST does not propagate with a uniform phase speed; a remarkable phase shift is observed in the area around 150–160°E, where the zonal wind anomalies at the 700 mb level have the largest amplitudes. Thus, the QBO mode of the tropical SST does not always propagate in parallel with that of the tropical lower troposphere. The tropical tropospheric QBO mode propagating eastward from the Indain Ocean brings about the remarkable phase shift in the SST anomalies around 150–160°E. It is inferred that these variations, which are affected by the accumulation and release of warm water east of the Philippines, result from the dynamic response of the ocean to the wind stress having a QBO variability since the QBO modes of the SST and upper ocean temperature are basically an identical phenomenon.

Intraseasonal time scale

The growth of atmospheric 30–60 day oscillation over the tropical western Pacific is influenced even by SSTs above a threshold value of 28°–28.5℃. The oscillation becomes predominant when the SST is around 29.3℃. Once the equatorial western Pacific SST is beyond the *upper threshold* value of about 29.5℃, it is clearly seen that the 30–60 day oscillation is damped in this region, while tropical large-scale convection is still rather active. As a consequence, high-frequency fluctuations become relatively dominant under high-SST conditions.

When the SST in the warm pool region is in the range between 29° and 29.5℃, the *oceanic* 30–60 day fluctuation is significant with the SST and large-scale convection fluctuating coherently on the intraseasonal time scale, having a phase difference of 10–20 days. The 30–60 day oscillation is presumably modified over the warm pool region of the western Pacific by strong air-sea interaction on the intraseasonal time scale.

Air–sea coupled modes on the two time scales

Using the CEOF analysis, two air-sea coupled modes; *i.e.*, the intraseasonal and interannual modes, are statistically extracted.

It is found that for the intraseasonal mode the area of maximum SST anomaly lies to the east of the center of the active large-scale convection area. This implies that positive SST anomalies exist in the easterly anomaly area, providing a favorable condition for a large-scale disturbance to propagate eastward. Also, the evaporation-wind feedback mechanism may favor its eastward propagation if the mean wind is easterly.

The interannual mode has a characteristic that the phase relation between the 850 mb u and the SST is different in each region of the tropical western Pacific whereas the SST is almost in phase with the high-

cloud cover. The predominant growth of the mode defined in the key region (0°–10°N, 130–160°E) corresponds to the life cycle of an ENSO event; genesis, development, and decay. This verifies that the ENSO is one of the prominent phenomena in the air–sea interactive system on the interannual time scale. The mode over the tropical Pacific around the dateline, on the other hand, shows a linear-like coupling of the atmosphere/ocean system when large-scale convection is not very active.

Intraseasonal air–sea coupling and ENSO

It is important for the precondition of warm ENSO events that the ocean heat content (OHC) in the western Pacific increases during the late autumn and winter one year prior to the mature phase of warm events (*e.g.*, Cane *et al.*, 1986; White *et al.*, 1987; Takeuchi, 1987). Very recently, Yamagata and Masumoto (1989) suggested that both increased OHC and westerly bursts in the warm pool region of the western Pacific are necessary as preconditions of warm events. It was furhter pointed out that the westerly bursts associated with the 30–60 day oscillation possibly act as triggers of the warm events (Nitta and

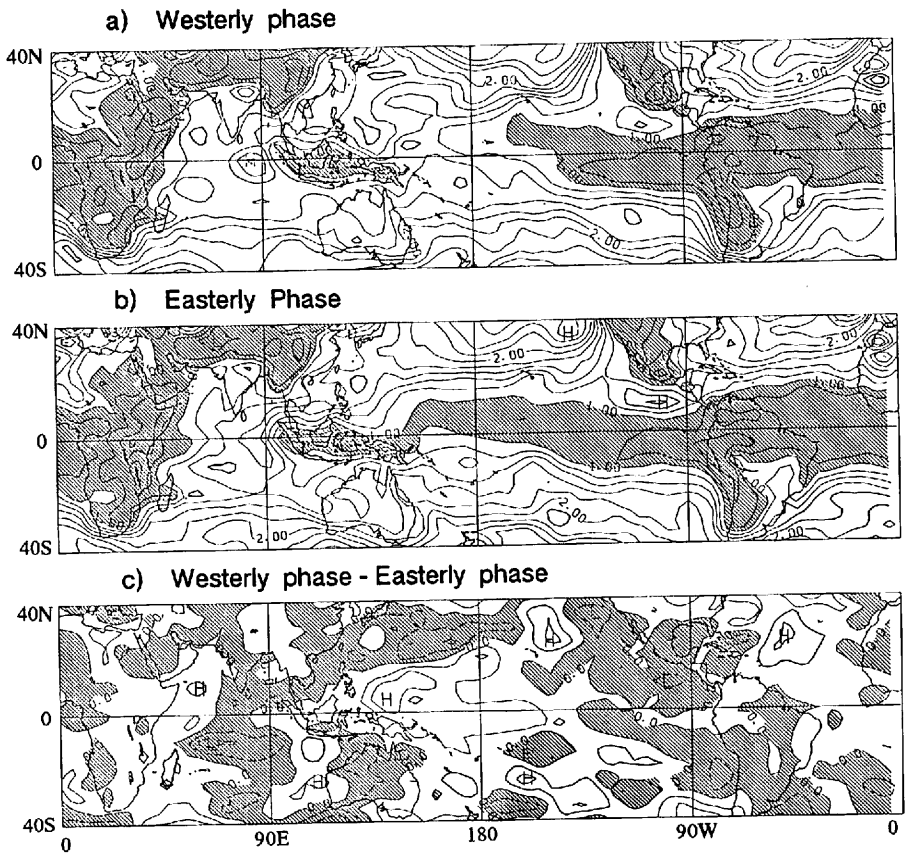

Fig.6.1 Composite intraseasonal amplitudes of 850mb u for the (a) westerly phase and (b) easterly phase of the interannual component in the key region (0°–10°N, 130–160°E). Contour interval is 0.2ms^{-1} and regions less than 1 ms^{-1} are shaded. (c) Differences of the intraseasonal amplitudes between both phases. Contour interval is 0.2ms^{-1} and negative anomaly areas are shaded.

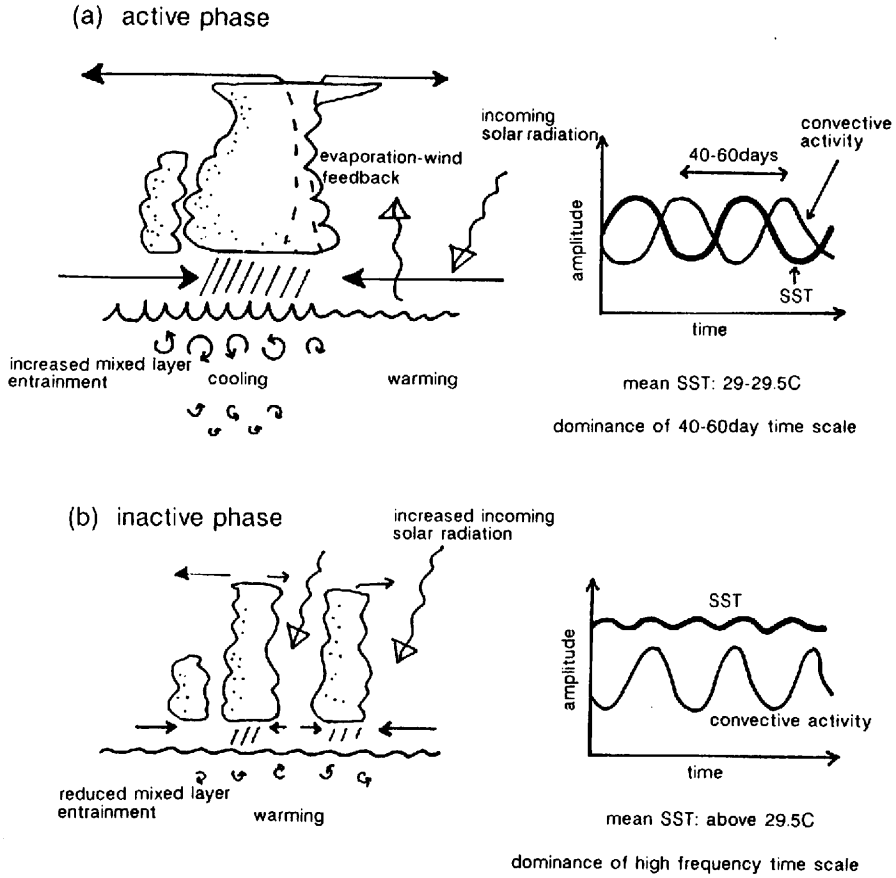

Fig.6.2 Schematic diagrams displaying (a) active phase and (b) inactive phase of the air–sea coupled system on the intraseasonal time scale.

Motoki 1987; Lau and Chan, 1986).

The 30–60 day oscillation was observed to be active over the western Pacific during the northern summers (May–October) of 1976, 1979, 1982, 1986 and 1987 (Fig. 4.6). The northern summers of 1976, 1982 and 1986 correspond to the periods just before the occurrences of warm events. Although the oscillation is dominant during the period of May–October 1987, this appears to be associated with the fact that the 1986/88 event persisted for about two years. However, the warm event did not occur during the period 1979/80 despite the dominance of the 30–60 day oscillation. If the QBO phase of 700 mb zonal wind anomaly (Fig. 3.9) is examined, the northern summers of 1976 and 1982 correspond to a westerly phase, while that of 1979 is equivalent to an easterly phase. Figure 6.1 shows the composite intraseasonal amplitudes of the 850mb u for the (a) westerly phase and (a) easterly phase of the interannual component over tne key region (0°–10°N, 130–160°E). It is seen that the intraseasonal amplitudes of the 850mb u are large in the western Pacific east of the Philippines. It can also be seen that significant differences in the intraseasonal amplitudes between the westerly and easterly phases (Fig. 6.1c). These results suggest that westerly bursts of the 30–60 day disturbances, which act as triggers of warm events, are presumably dominant near the key region. Furthermore, when the QBO mode has an easterly phase, the warm event barely occurs, even though the 30–60 day oscillation is active over the tropical western Pacific.

The above features are associated with the air-sea coupling on the intraseasonal time scale. Figure 6.2 schematically illustrates (a) the active phase and (b) inactive phase of the air-sea coupling on the intraseasonal time scale.

1) *active phase*. The mean SST over the warm pool region of the western Pacific is in the range between 29 to 29.5℃. The intraseasonal variations especially with a 40-60 day time scale are prominent. There exists a strong air-sea coupling on the intraseasonal time scale in the warm pool region. The region of maximum SST anomaly lies to the east of the center of the active convection area, which favors the eastward propagation of the disturbance as well as the evaporation-wind feedback effect presented by Emanuel (1987) and Neelin *et al.* (1987). The increased incoming solar radiation over the ocean surface contributes to the formation of positive SST anomalies in the easterly anomaly area. If the warm pool region is covered with a fresh lens (Lukas, 1988), it may be easy to warm the upper part of the ocean. The increased mixed-layer entrainment and reduced incoming solar radiation in the westerly anomaly area lead to a cooling of the underlying SST. However, it is considered that the cooling in the upper ocean requires strong turbulent mixing by large-scale disturbances, since the fresh lens effect stabilizes the upper ocean. Since the air-sea coupled system on the intraseasonal time scale moves eastward, the could-SST negative feedback mechanism does not work for diminishing clouds; rather, it may modify the period of the air-sea coupling on this time scale. The SST cooling due to the mixed-layer entrainment does not easily occur when the ocean mixed layer is very deep. Thus, when the OHC anomalies are maximized in the western Pacific, strong air-sea coupling on the intraseasonal time scale hardly exist. However, strong air-sea coupling may occur in the westerly phase of the QBO mode, when the maximized OHC anomalies gradually lessens. This may possibly become a trigger of warm ENSO events.

2) *inactive phase*. The mean SST is almost always beyond the upper threshold value of about 29.5℃. Although large-scale convection is still rather active, the 30-60 day oscillation is damped over the equatorial western Pacific and the high-frequency fluctuation is, as a result, relatively enhanced. The air-sea coupling in the 30-60 day time scale is very weak in this region and disturbances on the scale of organized super clusters are rarely observed. The reduced mixed layer entrainment can not cause the large-scale negative SST anomaly. Also, the remarkable eastward-moving air-sea interactive system can not be seen. This inactive phase tends to occur during the easterly phase of the QBO mode when the OHC increases and the mixed layer deepens in the tropical western Pacific.

ACKNOWLEDGEMENTS

The author is grateful to Professor M. Yoshino and Dr. T. Yasunari, University of Tsukuba, for their invaluable suggestions and encouragement throughout the present study. Special thanks are extended to Professor T. Kawamura and Professor T. Nishizawa, University of Tsukuba, for providing helpful comments, and to Professor I. Kayane, Director of Environmental Research Center, University of Tsukuba, for the publication of this thesis as an ERC Papers. The author is also indebted to Dr. Y. Hayashi of Geophysical Fluid Dynamics Laboratory, Princeton University, for reviewing the manuscript.

Thanks are extended to the staff of the Oceanographical Division and the Long-range forecasting Division of the Japan Meteorological Agency for making available oceanographical and meteorological data used in this study. The author also expresses his thanks to Dr. T. Nakazawa of the Meteorological Research Institute for his guidance and permissions for the use of his compiled OLR data. Thanks are further extended to the UK Meteorological Office for making available historical sea surface temperature data set. Acknowledgement is also made to Dr. H. Ikeda, Dr. J. Shimada, Dr. F. Iseya, Mr. H. Iijima and Mr. Y. Kodama of the Environmental Research Center. Heartfelt thanks are also to Ms. Y. Mizuta, Ms. M. Shinozaki and Ms. C. Kusama for many indirect supports.

This research was financially supported by the University of Tsukuba Project Research for 1989. Computations were performed with the FACOM M-780/20 at the Science Information and Processing Center of the University of Tsukuba.

REFERENCES

Arkin, P.A., J.D. Kopman and R.W. Reynolds, 1983: *1982–83 El Nino/Southen Oscillation Event Quick Look Atlas.* NOAA/NWS/NMC/Climatic Analysis Center.

Barnett, T.P., 1983: Interaction of the monsoon and Pacific trade wind system at interannual time scales, Part I, The equatorial zone. *Mon. Wea. Rev.*, **111**, 756–773.

Cane, M.A., S.E. Zebiak and S.C. Dolan, 1986: Experimental forecasts of El Nino. *Nature*, **321**, 827–832.

Chang, C.-P. and K.G. Lum, 1985: Tropical–midlatitude interactions over Asia and the western Pacific Ocean during the 1983/84 northern winter. *Mon. Wea. Rev.*, **113**, 1345–1358.

Chu, P.C. and R.W. Garwood, Jr., 1990: On the two-phase thermodynamics of the coupled cloud–ocean mixed layer. *Submitted to J. Geophys. Res.*

Emanuel, K.A., 1987: An air–sea interaction model of intraseasonal oscillations in the tropics. *J.Atmos. Sci,*. **44**, 2324–2340.

Enfield, D.B. and R.B. Lukas, 1984: Low frequency sea level variability along the South American coast in 1982–83. *Tropical Ocean–Atmosphere Newsletter*, **28**, 2–4.

Gadgil, S., P.V. Joseph and N.V. Joshi, 1984: Ocean–atmosphere coupling over monsoon regions. *Nature*, **312**, 141–143.

Graham, N.E. and T.P. Barnett, 1987: Sea surface temperature, surface wind divergence, and convection over tropical oceans. *Science*, **238**, 657–659.

Gutzler, D.S. and D.E. Harrison, 1987: The structure and evolution of seasonal wind anomalies over the near–equatorial eastern Indian and western Pacific Oceans. *Mon. Wea. Rev.*, **115**, 169–192.

Hanawa, K., T. Watanabe, N. Iwasaka, T. Suga and Y. Toba, 1988: Surface thermal condition in the western North Pacific during the ENSO events. *J. Meteor. Soc. Japan*, **66**, 444–455.

Hayashi, Y. and D.G. Golder, 1986: Tropical intraseasonal oscillations appearing in a GFDL general circulation model and FCGE data, Part I: Phase propagation. *J. Atmos. Sci.*, **43**, 3058–3067.

_____, 1988: Tropical intraseasonal oscillations appearing in a GFDL general circulation model and FGGE data, Part II: Structure. *J. Atmos. Sci.*, **45**, 3017–3033.

Hayashi, Y. Y. and A. Sumi, 1986: The 30–40 day oscillations simulated in an "aqua planet" model. *J. Meteor. Soc. Japan*, **64**, 451–467.

Hollingsworth, A., D.B. Shaw, P. Lonnberg, L.Illam, K. Arpe and A. J. Simmons, 1986: Monitoring of observations and analysis quality by a data assimilation system. *Mon. Wea. Rev.*, **114**, 861–879.

Kawamura, R., 1988a: The interaction between winter monsoon activities in East Asia and sea surface temperature variations over the western Pacific Ocean. *Geographical Review of Japan*, **61** (Ser. A), 469–484 (*in Japanese with English abstract*).

_____, 1988b: Intraseasonal variability of sea surface temperature over the tropical western Pacific. *J. Meteor Soc. Japan*, **66**, 1007–1012.

Krishnamurti, T.N., D.K. Oosterhof and A.V. Mehta, 1988: Air–sea interaction on the time scale of 30 to 50 days. *J. Atmos. Sci.*, **45**, 1304–1322.

Kutsuwada, K., 1988: Short-term climatic variations appearing in the sea level field of the western Pasific. *Marine Sciences Monthly*, **20**, 294–300 (*in Japanese*).

Lau, K.-M. and P.H. Chan, 1986: The 40–50 day oscillation and the El Nino/Southern Oscillation: A new perspective. *Bull. Amer. Meteor. Soc.*, **67**, 533–534.

_____. and L. Peng, 1987: Origin of low frequency (intraseasonal) oscillations in the tropical atmosphere, Part I: The basic theory. *J. Atmos. Sci.*, **44**, 950–972.

_____. and P.H. Chan, 1988: Intraseasonal and interannual variations of tropical convection: A possible link between the 40–50 day oscillation and ENSO? *J. Atmos. Sci.*, **45**, 506–521.

_____. and P.J. Sheu, 1988: Annual cycle, quasi-biennial oscillation and southern oscillation in global precipitation. *J. Geophys. Res.* (*to be published*)

_____. and S. Shen, 1988: On the dynamics of intraseasonal oscillations and ENSO. *J. Atmos. Sci.*, **45**, 1781–1797.

Lau, N.-C. and K.-M. Lau, 1986: The structure and propagation of intraseasonal oscillations appearing in a GFDL general circulation model. *J. Atmos. Sci.*, **43**, 2023–2047.

Lukas, R., 1988: On the role of western Pacific air–sea interaction in the El Nino/Southern Oscillation Phenomenon. In: *Proceedings of the U.S. TOGA Western Pacific Air–Sea Interaction Workshop Honolulu, 16–18 September, 1987. R. Lukas and P. Webster, eds., U.S. TOGA Rept. USTOGA–8, U. Corp. Atmos. Res.*, 43–69.

Meehl, G.A., 1987: The annual cycle and interannual variability in the tropical Pacific and Indian Ocean regions. *Mon. Wea. Rev.*, **115**, 27–50.

Miyahara, S., 1987: A simple model of the tropical intraseasonal oscillation. *J. Meteor. Soc. Japan*, **65**, 341–351.

Murakami, M., 1979: Large-scale aspects of deep convective activity over the GATE area. *Mon. Wea. Rev.*, **107**, 994–1013.

Murakami, T., 1988: Relationship between sea surface temperatures and outgoing longwave radiation on intraseasonal time scale. *Bull. Meteor. Soc. Japan (Tenki)*, **35**, 715–722 (*in Japanese*).

Mysak, L.A. and G.J. Mertz, 1984: A 40–60 day oscillation in the source region of the somali current during 1976. *J. Geophys. Res.*, **89**, 711–715.

Nakazawa, T., 1986: Intraseasonal variations of OLR in the tropics during the FGGE year. *J. Meteor. Soc. Japan*, **64**, 17–34.

Neelin, J.D., I.M. Held and K.H. Cook, 1987: Evaporation–wind feedback and low–frequency variability in the tropical atmosphere. *J. Atmos. Sci.*, **44**, 2341–2348.

Nitta, T. and T. Motoki, 1987: Abrupt enhancement of convective activity and low-level westerly burst during the onset phase of the 1986–87 El Nino. *J. Meteor. Soc. Japan*, **65**, 497–506.

Parker, D.E. and C.K. Folland, 1988: The Meteorological Office historical sea surface temperature data set. In: *Recent climatic change, S. Gregory, ed., Belhaven Press.*

Philander, S.G.H., T. Yamagata and R.C. Pacanowski, 1984: Unstable air–sea interactions in the tropics. *J. Atmos. Sci.*, **41**, 604–613.

Saiki, M., 1987: Interannual variation of the subtropical gyre in the western North Pacific. *Umi to Sora*, **63**, 1–13 (*in Japanese with English Abstract*).

Schott, F., M. Fieux, J. Kindle, J. Swallow and R. Zantopp, 1988: The boundary currents east and north of Madagascar, 2, Measurements and model comparisons. *J. Geophys. Res.*, **93**, 4963–4974.

Spillane, M.C., D.B. Enfield and J.S. Allen, 1987: Intra–seasonal oscillations in sea level along the west coast of the Americas. *J. Phys. Oceanoger.*, **17**, 313–325.

Sui, C.-H. and K.-M. Lau, 1989: Origin of low frequency (intraseasonal) oscillations in the tropical atomosphere, Part II: Structure and propagation of mobile wave–CISK modes and their modification by lower boundary forcings. *J. Atmos. Sci.*, **46**, 37–56.

Takahashi, M., 1987: A theory of the slow phase speed of the intraseasonal oscillation using the wave–CISK. *J. Meteor. Soc. Japan*, **65**, 43–49.

Takeuchi, K., 1987: *Geophys. Bull. Hokkaido Univ.*, **49**, 381–386.

TOGA COARE, 1989: *Science plan of a coupled ocean–atmosphere response experiment for the warm pool regions of the western Pacific.* 111p.

Trenberth, K.E., 1975: A quasi–biennial standing wave in the southern hemisphere and interrelations with sea sur-

face temperature. *Quart. J. Roy. Met. Soc.*, **101**, 55–74.

Trenberth, K.E., and J.G. Olson, 1988: An evaluation and intercomparison of global analyses from the National Meteorological Center and the European Centre for Medium Range Weather Forecasts. *Bull. Amer. Meteor. Soc.*, **69**, 1047–1057.

Wang, X.-L. and T. Murakami, 1987: Intraseasonal meridional surges and equatorial convections during the southern hemisphere summer. *J. Meteor. Soc. Japan*, **65**, 727–736.

White, W.B., S.E. Pazan and M. Inoue, 1987: Hindcast/forecast of ENSO events based upon the redistribution of observed and model heat content in the western Pacific, 1964–86. *J. Phys. Oceanogr.*, **17**, 264–280.

Yamagata, T., 1987: A simple moist model relevant to the origin of intraseasonal disturbances in the tropics. *J. Meteor. Soc. Japan*, **65**, 153–165.

Yamagata, T and Y. Masumoto, 1989: A simple ocean-atmosphere coupled model for the origin of a warm El Nino Southern Oscillation event. *Phil. Trans. R. Soc. Lond.*, A **329**, 225–236.

Yasunari, T., 1985: Zonally propagating modes of the global east-west circulation associated with southern oscillation. *J. Meteor. Soc. Japan*, **63**, 1013–1029.

Yasunari, T., 1989: A possible link of the QBOs between the stratosphere, troposphere and sea surface temperature in the tropics. *J.Meteor. Soc. Japan*, **67**, 483–493.

Yasunari, T., 1989: Impact of Indian monsoon on the coupled atmosphere/ocean system in the tropical Pacific. *J. Climate (to be pubilshed)*.

Yoshino, M. and R. Kawamura, 1987: Periodicity and propagation of sea surface temperature fluctuations in the equatorial Pacific. *Beitr. Phys. Atmosph.*, **60**, 283–293.

Environmental Research Center Papers

No.1 (1982) Kenji KAI: Statistical characteristics of turbulence and the budget of turbulent energy in the surface boundary layer. 54p.

No.2 (1983) Hiroshi IKEDA: Experiments on bedload transport, bed forms, and sedimentary structures using fine gravel in the 4-meter-wide flume. 78p.

No.3 (1983) Yousay HAYASHI: Aerodynamical properties of an air layer affected by vegetation. 54p.

No.4 (1984) Shinji NAKAGAWA: Study on evapotranspiration from pasture. 87p.

No.5 (1984) Fujiko ISEYA: An experimental study of dune development and its effect on sediment suspension. 56p.

No.6 (1985) Akihiko KONDOH: Study on the groundwater flow system by environmental tritium in Ichihara region, Chiba Prefecture. 59p.

No.7 (1985) Chong Bum LEE: Modeling and climatological aspects of convective boundary layer. 63p.

No.8 (1986) Kazuo KOTODA: Estimation of river basin evapotranspiration. 66p.

No.9 (1986) Abdul Khabir ALIM: Experimental studies on transient behavior of capillary zone. 76p.

No.10 (1987) Michiaki SUGITA: Evaporation from a pine forest. 61p.

No.11 (1987) Hye-Sock PARK: Variations in the urban heat island intensity affected by geographical environments. 79p.

No.12 (1988) Hiroshi IKEDA and Fujiko ISEYA: Experimental study of hetergeneous sediment transport. 50p.

No.13 (1989) Hitoshi TORITANI: A local climatological study on the mechanics of nocturnal cooling in plains and basins. 62p.

No.14 (1990) Ryuichi KAWAMURA: Large-scale air-sea interactions in the tropical western Pacific on interannual and intraseasonal time scales. 64p.

発行　　平成2年12月1日
編集・発行者　筑波大学水理実験センター

〒305 つくば市天王台1－1－1
TEL 0298(53)2532 FAX (53)2530

印刷　ニッセイエブロ株式会社
東京都港区西新橋2－5－10